Circuit and Electromagnetic System Design Notes

Note 18

MATCHING A PARTICULAR PULSER TO A PARALLEL-PLATE SIMULATOR

R. W. Latham
M. I. Sancer
A. D. Varvatsis

Tetra Tech, Inc.
Pasadena, California

November 1974

Abstract

An electromagnetic energy source that incorporates the peaking capacitor arms of a Marx generator as part of its electromagnetic configuration is to be used in an Electromagnetic Pulse simulator to be built under the supervision of the Air Force Weapons Laboratory. In this report, the positions of the peaking capacitors that fulfill certain desirable null-flux conditions are determined. The characteristic impedance and several other useful properties of the conical base of the pulser are also calculated.

PREFACE

The purpose of the work reported here is to provide design data, derived through analysis and parametric study, to help to optimize the electromagnetic configuration of the pulser that is to be used in the ATLAS EMP simulator facility. Sufficient variation of the parameters of the configuration have been included to optimize the performance of the pulser in both the Pulser Test Fixture (PTF) and the horizontal simulator of the ATLAS facility.

The authors acknowledge the usefulness of the technical discussions of this problem with Dr. C. E. Baum of the Air Force Weapons Laboratory.

CONTENTS

ILLUSTRATIONS

TABLES

SECTION I

INTRODUCTION AND SUMMARY

The energy source for the ATLAS electromagnetic pulse (EMP) simulators will be a little different from previous energy sources for stationary simulators in that the peaking capacitor arms of the Marx generator will be incorporated as part of the electromagnetic parallel-plate wave guiding configuration of the system. Since it is effectively a piece of the transmission line guiding the simulation pulse, it must satisfy the primary criterion for every portion of such a line, i. e., it must have the same characteristic impedance as every other portion of the line. This criterion, although impossible to satisfy exactly because of difficulties in both analysis and construction, should be satisfied as closely as possible if one hopes for small reflections (little ringing) caused by the transmission line sections themselves. The reflections caused by the presence of a test object are another matter and are the inevitable result of the process of simulation. But reflections in the absence of a test object must be minimized as much as possible in order to ensure as accurate a simulation as is possible with the given energy source and to minimize the wasted energy.

Thus, we are induced to determine just what is the characteristic impedance of each section of the transmission-line simulator. In the present case there are two major sections of the transmission-line simulator (sections of the pulser) for which the previously available numerical data on characteristic impedance is rather sparse. One purpose of the work reported here is to remedy that defect. The two sections we speak of are shown schematically in Figure 1 and consist of: (a) the base of the pulser, which takes the form of a monocone on a ground plane and (b) the four Marx generator peaking capacitor arms, when these arms are at the stage in the generation cycle such that they form a portion of the transmission-line.

The mere satisfaction of constant characteristic impedance along the line does not uniquely determine the parameters of either the

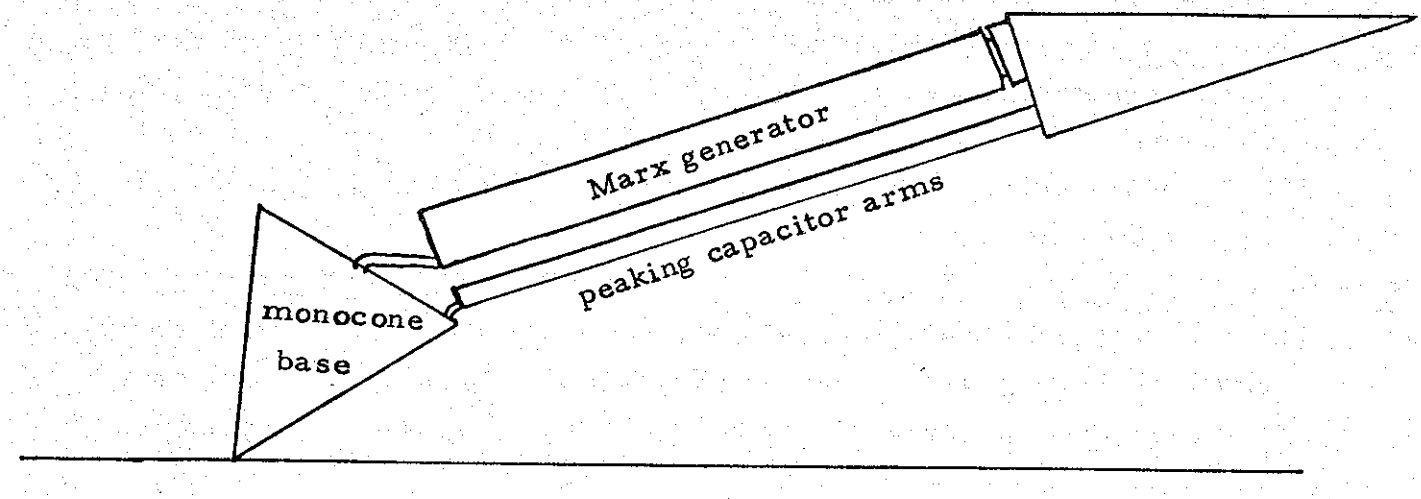

a side view

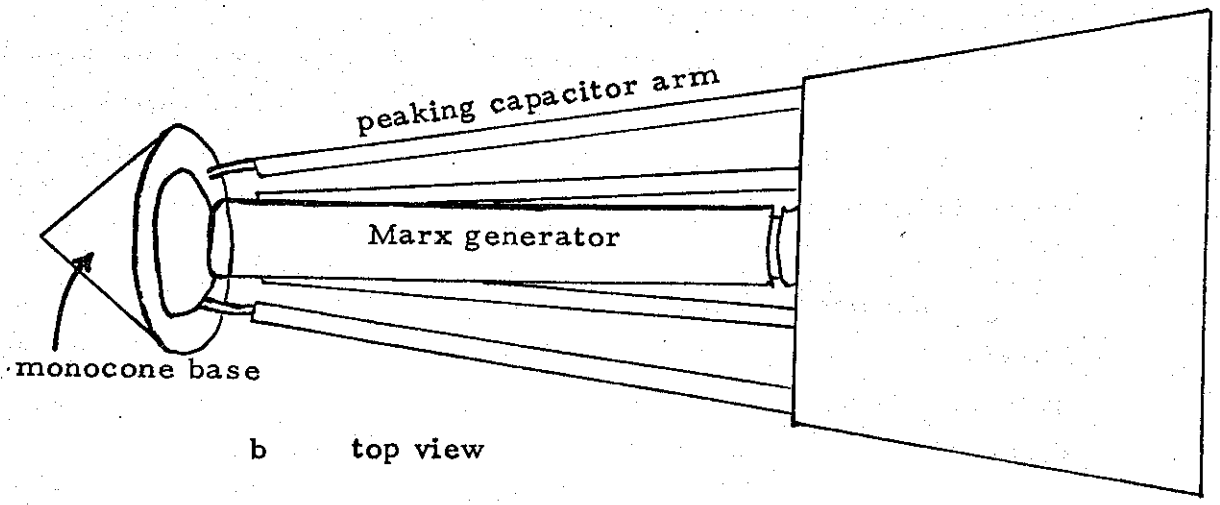

b top view

Figure 1: Schematic pulser configuration

monocone section or the capacitor arm section. This can be seen, for example, in Section II, when pairs of values of the monocone parameters (cone angle and tilt angle) lead to the same characteristic impedance. Thus, we have some freedom in the choice of pulser parameters which we can use to optimize some other aspect of its electromagnetic performance besides the dominant reflection minimizing criterion of constant characteristic impedance. Therefore, we are led to a more extensive study of the pulser sections than would suffice for just a characteristic impedance calculation.

In particular, for the monocone section we can consider that it should produce a transverse field distribution that matches, as closely as is feasible, the next section of line it is feeding into. Alternatively we could consider reducing the back radiation as much as possible. This reduction does not necessarily work in opposition to the production of good field distributions; in fact the two things seem to go together. For the capacitor arm section, since it is desirable to reduce the voltages between arms as much as possible both in the capacitor charging stage (when the return current is through the Marx generator) and the discharging stage (when the four arms act like the top plate of a parallel-plate transmission line and the return current can be thought of as flowing in the images of the arms in the ground plane) we can consider those configurations that result in zero net flux between any pair of arms under one or both of the conditions on return current. We will now consider these topics in a little more detail.

The monocone on a groundplane can, by invoking the theory of images, be thought of as a symmetrical bicone. Such structures have been studied extensively theoretically (reference 1 contains much of this analysis), primarily as an approach to the analysis of thin wire radiating antennas. As a consequence, any numerical data that has previously existed has been almost entirely restricted to the case where

---

1. Schelkunoff, S. A., Advanced Antenna Theory, John Wiley and Sons, Inc., New York, 1952.

the monocone axis is vertical (when translated back to our terms). Thus, the first order of business in the monocone analysis will be to produce data on the characteristic impedance of a tilted monocone conical transmission line. This will be done in Section II. 1. The results of this calculation, given in Section II, show that to attain the high impedances sometimes contemplated for ATLAS the monocone half-angle must be rather small (less than 20°), but that the monocone can be tilted considerably. An example of a 140-ohm line would be a monocone with a 10° half-angle tilted 25° from the vertical.

Another subject on which previous quantitative data is nonexistant is the distribution of the electric and magnetic fields over the spherical wavefronts of the conical line. This information is of use in trying to pick that monocone tilt angle which will produce field distribution most closely matching those in the cross sections of other sections of the simulator. It is straight forward to derive explicit equations for the field lines on the wavefront. This is done in Section II. 2. The problem of the useful pictorial presentation of the field-line data has been solved by drawing pictures of how the lines would look if they were painted on a sphere and then looked at from the front (i.e., looking back toward the apex of the cone). These pictures are given in Section II. From these pictures we see that the transverse homogeneity of the field increases as the monocone becomes more vertical, but against this we must oppose the reminder that the curvature of the lines under the monocone (those primarily involved in injecting energy into the simulator) become more curved, as viewed from the side view, as the monocone approaches verticality. A reasonable compromise would seem to be to have the monocone tilt about 20° or 30° from the vertical. Of course, when we speak of "vertical" in these remarks we mean the direction of the normal to the groundplane. The groundplane itself could have a slope within the pulser section.

The last aspect of the monocone portion of the structure that we will look at is that of back radiation. An analysis of back radiation is given in Section II. 3 under the assumption that the monocone is in-

finitely long. Such an assumption will lead to an upper bound on the back radiation since the rest of the simulator structure will tend to direct more of the energy forward than an infinite monocone at a realistic angle. Nevertheless, the analysis shows that for reasonable monocone half-angles and angles of tilt the energy radiated back into the entire rear hemisphere cannot exceed 10% or 20% of the total energy radiated (18% for a 10° half-angle cone tilted 25° from the vertical).

The importance of minimizing voltages between capacitor arms in the section of the source where they dominate the electromagnetic configuration dictates that we should determine those configurations that result in zero flux between any pair of arms first, calculating characteristic impedances only after suitable geometrical arrangements are found. The desired configurations are all symmetrical about a vertical plane through the Marx generator. In Section III. 1 we treat the case where the peaking capacitors are charging and the return current flows through the Marx. It is found that by fixing the position of the outer pair of the four capacitor arms, the null flux condition requires that the inner arms must lie along a certain line in the cross-sectional plane. Plots of the inner arm trajectories are given as Figures 11 and 12. There are planar configurations of the four arms in the present case, which may be an advantage from the constructional point of view, but these become unavailable (and perhaps irrelevant) if we must also have zero net flux for the second condition on the return current (i. e. through image arms).

The case of image-arm return current is handled in Section III.2. This analysis is applicable when the peaking capacitors are discharging. Again it is found that, when viewed in cross section for a fixed position of the outer pair of arms, the inner arms must fall on a certain line. Plots of such trajectories are given in Section III.

There are geometrical configurations that satisfy the null flux requirement under both conditions on the return current simultaneously. This subject is treated in Section III. 3. It is found that for any position

of the outer pair of capacitor arms (within certain, not very restirctive, limits) there is a unique position for the inner pair of arms such that there is no arm-linking flux either with a Marx return current or with image arm return current. These inner arm positions can be found in Section III. To be able to fully use the results shown graphically in Section III, the reader is referred to the paragraphs describing them, where an example of their use may also be found. There is a rather wide latitude of choice in arm positions even when both null flux conditions are imposed, but none of these choices lead to a planar configuration.

Some minor points on the analysis, of the nature of explicit or implicit assumptions and their justification, may be found in Section IV.

SECTION II

TILTED MONOCONES ON A GROUND PLANE

1. IMPEDANCE

To analyze a tilted monocone on a ground plane, set up the coordinate system and the notation as shown in Figure 2. The angle of the axis of the monocone above the ground plane will be denoted by α and the half-angle of the monocone itself will be denoted by β. A spherical coordinate system will be used. The pole of the spherical coordinate system lies along the projection of the monocone axis on the ground plane. The $\varphi = 0$ plane is the ground plane. Clearly, in this coordinate system, the equation of the surface of the monocone becomes

$$\cos\theta \cos\alpha + \sin\theta \sin\alpha \sin\varphi = \cos\beta \tag{1}$$

The characteristics of the TEM mode wave propagation along the transmission line made up of the monocone. The ground plane can be determined by solving a surface Laplace equation over a spherical surface orthogonal to the direction of wave propagation. The surface Laplace equation over a sphere can be reduced to the usual two dimensional Laplace equation by the method of stereographic projection (see, for example, references 2 and 3).

Putting the above statements into more precise form, it can be shown (for example, in reference 2, Section 14.07) that the TEM mode electric field in a conical transmission line takes the form

$$\underline{E} = \frac{e^{\pm ikr}}{r} \nabla_t U(\theta, \varphi) \tag{2}$$

---

2. Smythe, W. R., Static and Dynamic Electricity, McGraw-Hill Book Co., Inc., New York, 1950.
3. Baum, C. E., "The conical transmission line as a wave launcher and terminator for a cylindrical transmission line", AFWL Sensor and Simulation Notes, Note 31, January 1967.

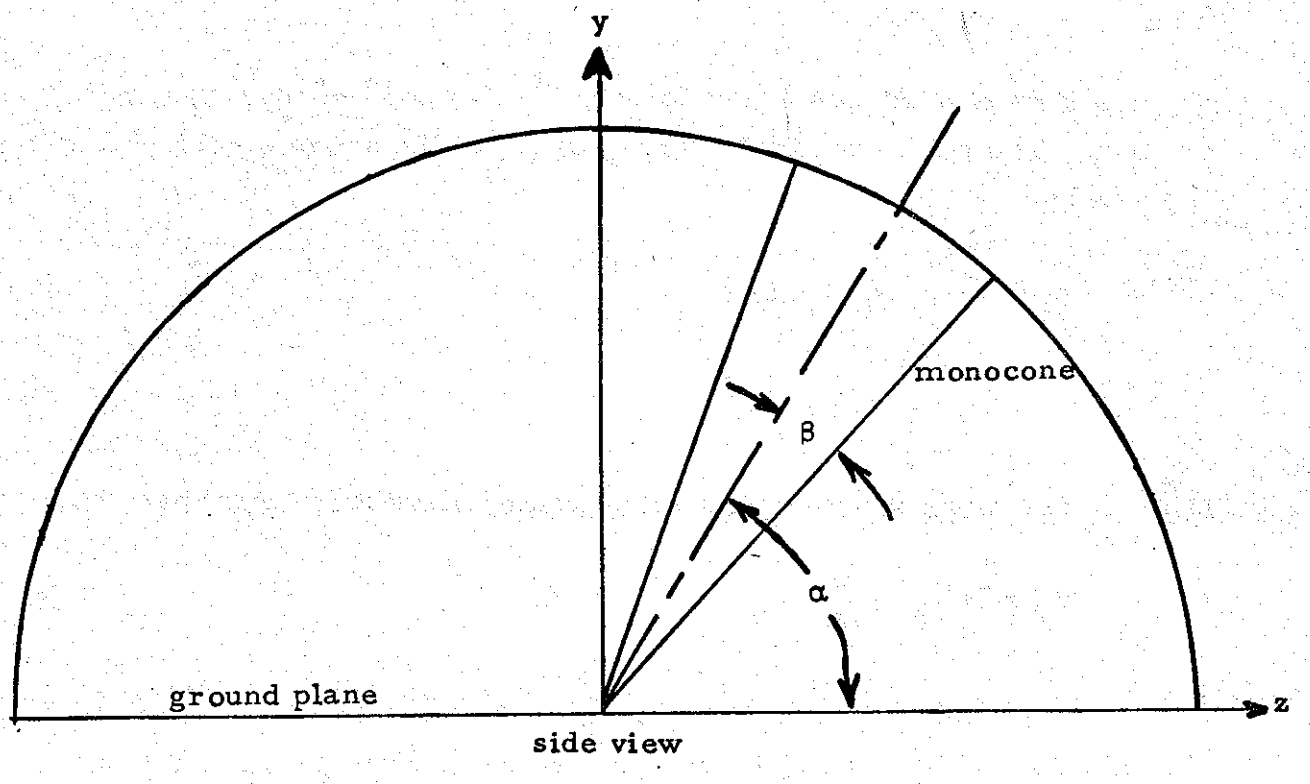

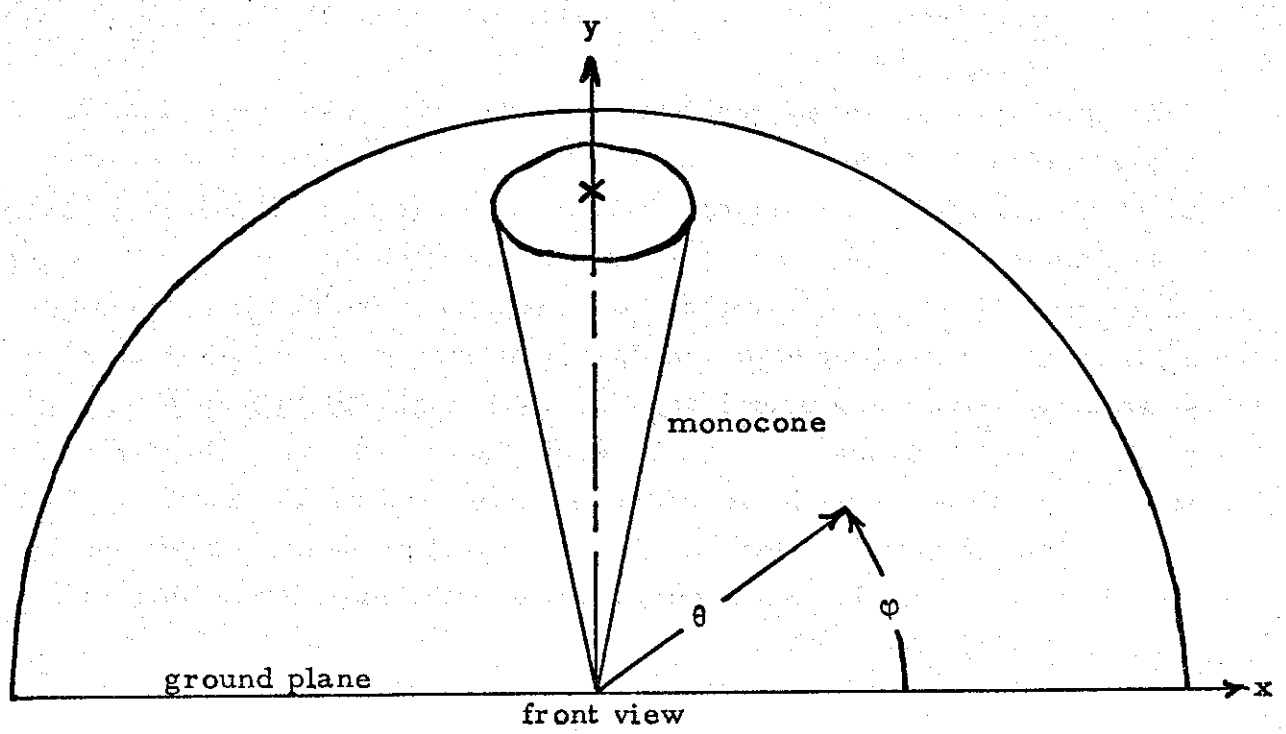

Figure 2: Monocone notation and coordinate system

where a time dependance of the form $e^{-i\omega t}$ has been suppressed and $k = \omega/c$. The magnetic field corresponding to the above electric field is given by

$$\underline{H} = \frac{\pm e^{\pm ikr}}{Z_o r} \underline{e}_r \times \nabla_t U(\theta, \varphi)$$

$$= \frac{\pm e^{\pm ikr}}{Z_o r} \nabla_t V(\theta, \varphi) \qquad (3)$$

In these equations ∇_t is a transverse gradient given explicitly by

$$\nabla_t \equiv \underline{e}_\theta \frac{\partial}{\partial \theta} + \frac{\underline{e}_\varphi}{\sin\theta} \frac{\partial}{\partial \varphi} \qquad (4)$$

The combination U+iV is an analytic function of the variable $e^{i\varphi}\tan(\theta/2)$. This fact can be used to set up an equivalent cylindrical transmission line for which the cross-section coordinates are

$$x' = \cos\varphi \tan\theta/2 \quad , \quad y' = \sin\varphi \tan \theta/2 \qquad (5)$$

This amounts to a stereographic projection. If we can determine the characteristics of the equivalent cylindrical transmission line formed by stereographic projection of our conical line (i. e., if we can solve the two-dimensional Laplace equation in the projected plane), the properties of the conical line (for example, the equations of the electric and magnetic field lines) follow from simple transformations. In particular, it is easy to show, using equations (2) and (3), that the characteristic impedances of the conical line and its equivalent are equal. The determination of this characteristic impedance will be our first calculation. This calculation appears in reference 2, but we will present it here because we will need to develop it further, a little later, in order to obtain the equations of the field lines.

The equation of the ground plane, $\varphi = 0$, becomes in the projected plane, according the equation (5)

$$y' = 0 \qquad (6)$$

The equation of the monocone, given as equation (1) becomes in the projected plane, where $\rho^2 = x'^2 + y'^2$,

$$\frac{1 - \rho^2}{1 + \rho^2} \cos \alpha + \frac{2 \sin\alpha}{1 + \rho^2} \rho \sin\varphi = \cos \beta \tag{7}$$

which, by simple algebraic manipulation can be rewritten

$$\rho^2 + \rho_o^2 - 2 \rho\rho_o \sin\varphi = R^2 \tag{8}$$

where

$$\rho_o = \frac{\sin\alpha}{\cos\beta + \cos\alpha} \tag{9}$$

and

$$R = \frac{\sin\beta}{\cos\beta + \cos\alpha} \tag{10}$$

Equation (8) is the equation of a circle of radius R whose center is on the y'-axis and at a distance ρ_o from the origin. But equation (1) can be thought of as the equation of any circle on a sphere and so it is seen that circles transform into circles by stereographic projection. This fact will be very useful a little later when we come to plotting field lines. For the moment, however, we are only interested in the fact that our monocone-groundplane conical line has transformed into a circular cylinder above a groundplane by stereographic projection. The characteristic impedance of such a structure is well known (see, for example, reference 2, Section 14. 14) to be

$$Z = \frac{Z_o}{2\pi} \cosh^{-1}\left(\frac{\rho_o}{R}\right) \tag{11}$$

According to our previous discussion this is also the impedance of the monocone. If we substitute the monocone parameters using equations (9) and (10), and if we also say $Z_o \approx 120\pi$ we obtain for the impedance

we desired to calculate,

$$Z = 60 \cosh^{-1} (\sin\alpha / \sin\beta) \tag{12}$$

This function of α and β is tabulated in Table 1 for $\beta = 5^{\circ}(5^{\circ})\ 50^{\circ}$ and $\alpha = 5^{\circ}(5^{\circ})\ 90^{\circ}$ where, of course, α must be greater than β.

The required α to give a certain impedance, Z, when β assumes various values, is given in Table 2, where missing values are unrealizable. The parameter range is $\beta = 5^{\circ}(5^{\circ})\ 50^{\circ}$ and Z = 10(10) 180 ohms. The equation used to calculate Table 2 comes from a simple flip of equation (12) and can be written as

$$\alpha = \sin^{-1} \left\{ \sin\beta \cosh \frac{Z}{60} \right\} \tag{13}$$

The impedance data is also displayed graphically in Figure 3. As can be seen from Figure 3, the $Z(\alpha)$ curves have vertical asymptotes as α approaches β and horizontal asymptotes as α appeoaches 90°. This can also be seen analytically by differentiating equation (12) to give

$$\frac{dZ}{d\alpha} = \frac{60 \cos\alpha}{\sqrt{\sin^2\alpha - \sin^2\beta}} \tag{14}$$

An interesting point about this data is that, in order to obtain impedances of around 150 ohms, one needs a half-cone angle of less than 10 degrees. With a 30 degree cone the impedance is less than 80 ohms.

2. FIELD DISTRIBUTION

We now turn to determining some of the properties of the electric and magnetic field distributions over a spherical surface. From what we have already said, it is clear that the TEM mode fields lie along concentric spherical surfaces and can be found by an appropriate transformation of the field lines of the equivalent transmission

TABLE 1

Impedance of a Tilted Monocone (in ohms)

$\alpha \backslash \beta$	5	10	15	20	25	30	35	40	45	50
5	0									
10	78.8	0								
15	105.1	57.2	0							
20	122.6	78.0	46.9	0						
25	135.7	92.2	64.4	40.4	0					
30	145.9	103.1	76.6	55.7	35.8	0				
35	154.3	111.9	86.0	66.4	49.3	32.2	0			
40	161.2	119.0	93.6	74.7	58.9	44.3	29.2	0		
45	167.0	124.9	99.8	81.3	66.2	52.9	40.2	26.6	0	
50	171.8	129.9	104.9	86.7	72.1	59.4	47.9	36.6	24.3	0
55	175.9	134.0	109.2	91.2	76.8	64.6	53.7	43.5	33.3	22.2
60	179.2	137.4	112.7	94.8	80.7	68.8	58.3	48.7	39.5	30.3
65	182.0	140.2	115.5	97.8	83.8	72.1	61.9	52.6	44.0	35.8
70	184.1	142.4	117.8	100.1	86.2	74.7	64.6	55.7	47.4	39.7
75	185.8	144.1	119.5	101.9	88.1	76.6	66.7	57.9	49.9	42.5
80	187.0	145.2	120.7	103.1	89.4	78.0	68.1	59.4	51.6	44.3
85	187.6	145.9	121.4	103.9	90.1	78.8	69.0	60.3	52.6	45.4
90	187.9	146.2	121.7	104.1	90.4	79.0	69.3	60.6	52.9	45.8

TABLE 2

Required α for a Given Z and β (Z in ohms)

Z/β	5	10	15	20	25	30	35	40	45	50
10	5.06	10.14	15.21	20.29	25.37	30.46	35.56	40.67	45.80	50.96
20	5.28	10.57	15.86	21.17	26.51	31.87	37.28	42.75	48.31	54.00
30	5.64	11.29	16.97	22.69	28.46	34.32	40.30	46.45	52.88	59.75
40	6.16	12.34	18.57	24.89	31.34	37.97	44.90	52.28	60.48	70.51
50	6.85	13.74	20.73	27.89	35.31	43.15	51.68	61.55	75.28	
60	7.73	15.54	23.54	31.85	40.70	50.49	62.26	82.69		
70	8.83	17.81	27.12	37.04	48.11	61.72				
80	10.18	20.63	31.67	43.93	59.02					
90	11.83	24.11	37.51	53.57	83.81					
100	13.82	28.43	45.20	69.67						
110	16.23	32.84	56.11							
120	19.14	40.79	76.84							
130	22.67	50.16								
140	26.98	64.66								
150	32.31									
160	39.06									
170	48.03									
180	61.34									

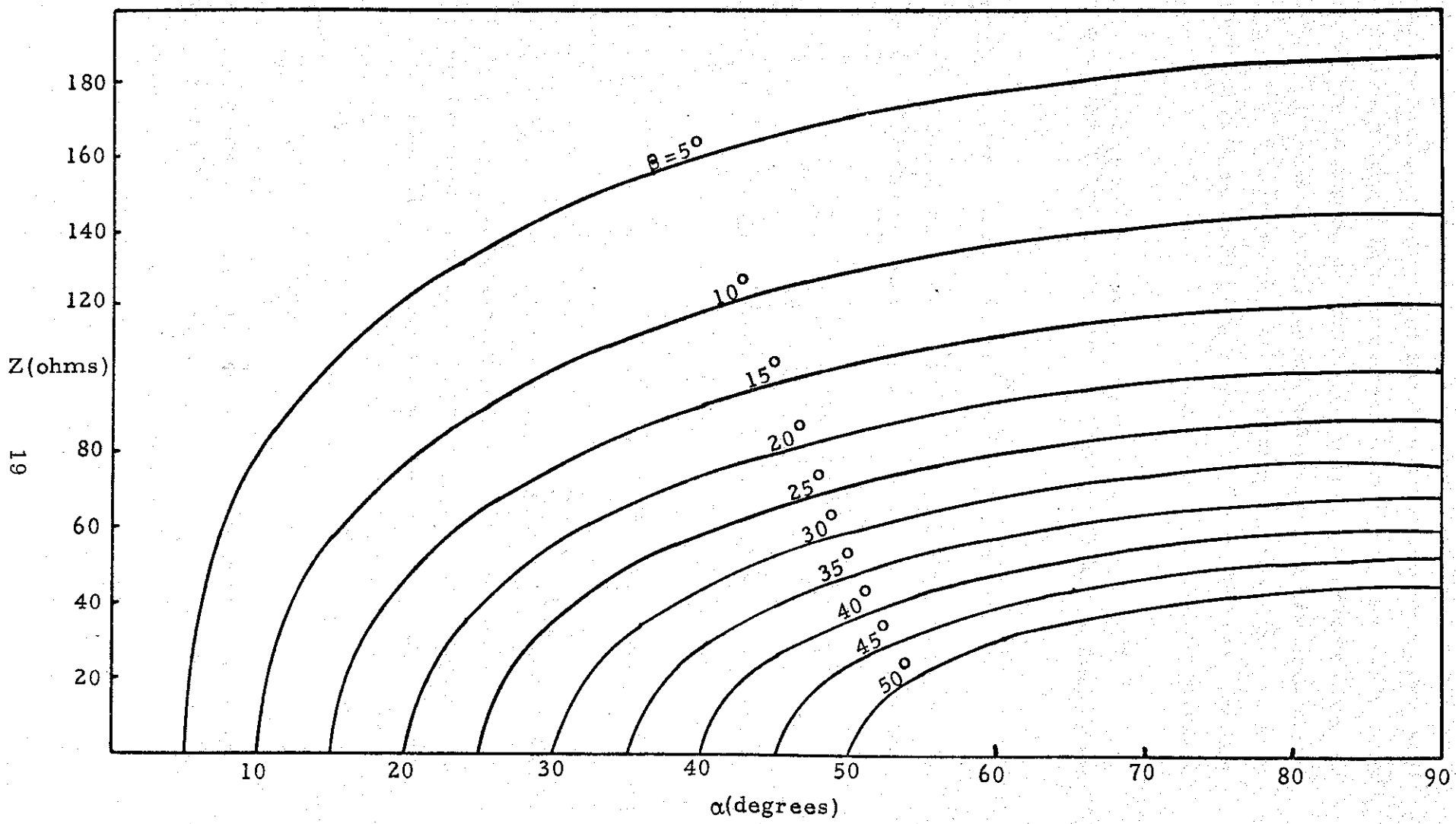

Figure 3: Impedance of a tilted monocone

line. From an examination of the two-cylinder transmission-line solution, it can be seen that all monocones that transform into cylinders having the same pole position (i. e., the same position of the effective line charge within the cylinder) have identical field distributions. Therefore, we can economize in our data presentation by plotting the fields with only the pole position (when transformed back to the spherical coordinate system) as a parameter.

The constant -V lines are given, in the projected plane, by (reference 2, Section 4. 13)

$$\rho^2 - 2a\rho \cos\varphi \cot V = a^2 \tag{15}$$

where the pole is at 0 + ia. If this pole is the projection of a conical pole at ($\theta = \theta_\rho$, $\varphi = \pi/2$), equation (15) can be rewritten as

$$\rho^2 + \rho_v^2 - 2\,\rho\rho_v \cos(\varphi-\varphi_o) = R_v^2 \tag{16}$$

where φ_o is 0 or π, according to whether cotV is greater or less than zero, and

$$\rho_v = \tan\left(\frac{\theta_\rho}{2}\right)\left|\cot V\right| \tag{17}$$

$$R_v = \tan\left(\frac{\theta_\rho}{2}\right)\left|\csc V\right| \tag{18}$$

Equation (16) represents a circle and so, from our previous demonstration that circles transform into circles by a stereographic projection or its inverse, we can say immediately that the equation of the V lines on the spherical surface is given by

$$\cos\theta \cos\theta_v + \sin\theta \sin\theta_v \cos(\varphi-\varphi_o) = \cos\gamma_v \tag{19}$$

where (θ_v, φ_o) are the angular coordinates of the center of the circle on the sphere and γ_v is the angular radius of that circle. To determine θ_v and γ_v we can note, from the analysis leading to equation (8)

and (9) that

$$\rho_v = \frac{\sin\theta_v}{\cos\gamma_v + \cos\theta_v} \tag{20}$$

$$R_v = \frac{\sin\gamma_v}{\cos\gamma_v + \cos\theta_v} \tag{21}$$

Solving these equations for θ_v and γ_v in terms of ρ_v and R_v we obtain, after a little algebra,

$$\tan\theta_v = \frac{-2\rho_v}{\rho_v^2 - R_v^2 - 1} \tag{22}$$

and

$$\tan\gamma_v = \frac{2Rv}{\rho_v^2 - R_v^2 + 1} \tag{23}$$

or, substituting the values of ρ_v and R_v from equations (17) and (18)

$$\tan\theta_v = \sin\theta_p \left|\cot V\right| \tag{24}$$

$$\tan\gamma_v = \tan\theta_p \left|\csc V\right| \tag{25}$$

When these values of θ_v and γ_v are used in equation (19) the result, after a little simplification, is

$$\cos\theta = \cos\theta_p - \sin\theta_p \cot V \sin\theta \cos\varphi \tag{26}$$

where we have used the fact that

$$\left|\cot V\right| \cos(\varphi - \varphi_o) = \cot V \cos\varphi \tag{27}$$

In a manner precisely analogous to our development of equation (15) into equation (26), we can proceed from the corresponding

equation for the U lines in the projected plane,

$$\rho^2 - 2a\rho \sin\varphi \coth U + a^2 = 0 \tag{28}$$

to the following equation for the U-lines in the (θ, φ) coordinate system

$$\cos\theta \cos\theta_p = 1 - \sin\theta_p \coth U \sin\theta \sin\varphi \tag{29}$$

The problem of a decent pictorial representation of the information contained in equations (26) and (29) now arises. One possibility would be a polar plot on a $(\rho';\varphi')$ plane, where $\rho' = \theta$ and $\varphi' = \varphi$, of the constant U and V lines. Another possibility would be some sort of Mercator projection of the spherical surface. We have chosen, however, for reasons of simplicity (and hopefully for reasons of maximum insight), to draw the field lines as they might actually be viewed from a given direction. That is to say, imagine the constant U and V lines to be painted on a spherical ball. Now look at this ball in a direction parallel to the projection of the monocone axis on the ground plane and toward the apex of the monocone. The result will be the pictures shown as Figures 4 through 9 for $\theta_p = 15^\circ(15^\circ)\,90^\circ$.

The equations for the U and V lines in these pictures are easily derived. In fact, using the relations

$$x = \sin\theta \cos\varphi \tag{30}$$

$$y = \sin\theta \sin\varphi \tag{31}$$

equation (26) reduces quite readily to

$$\left(\frac{x-x_v}{b_v}\right) + \frac{y^2}{a_v^2} = 1 \tag{32}$$

where

$$x_v = \frac{\sin\theta_p \cos\theta_p \sin V \cos V}{\sin^2 V + \sin^2\theta_p \cos^2 V} \tag{33}$$

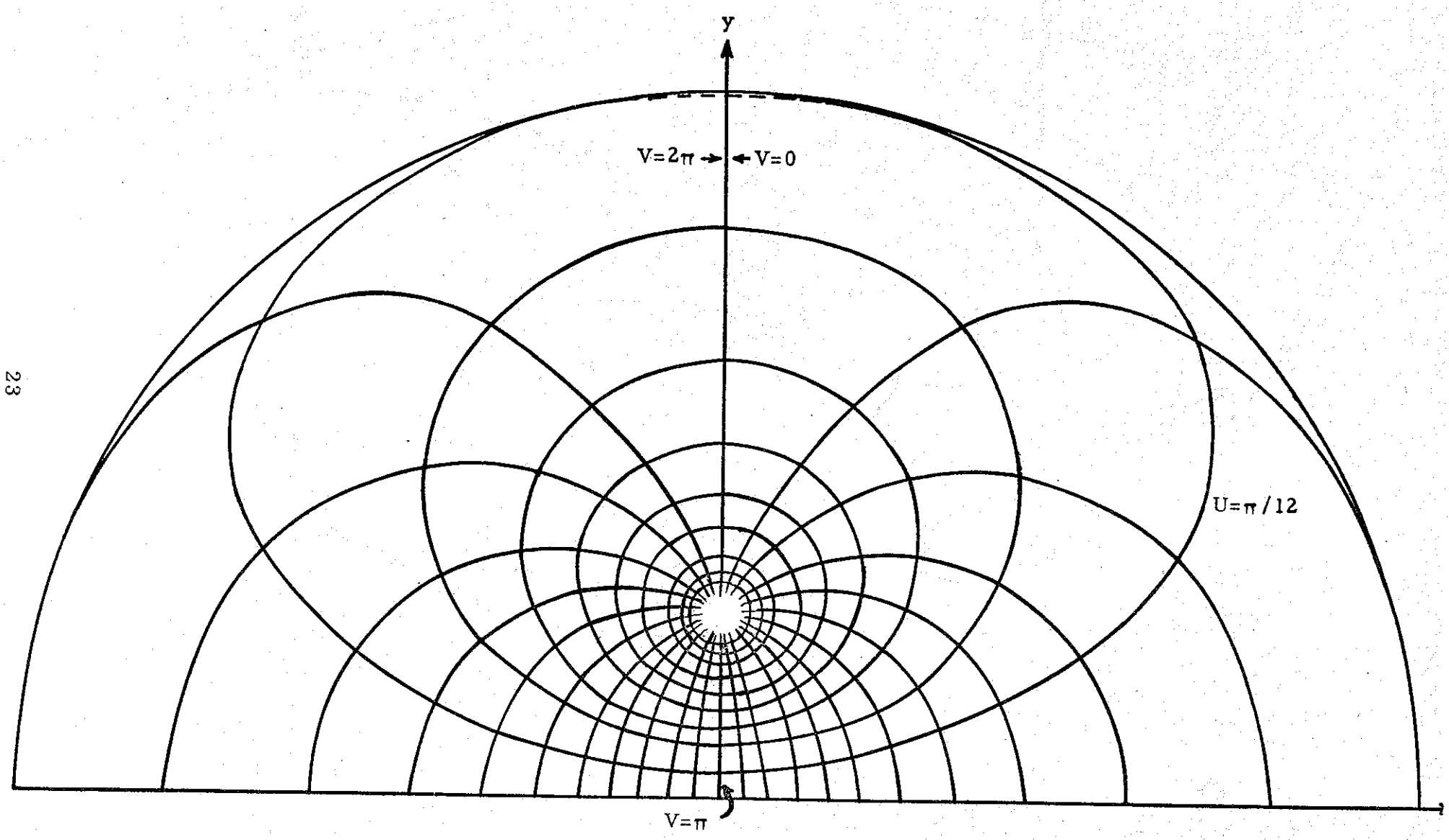

Figure 4: A view of the U-V lines for $\theta_p = 15^o$

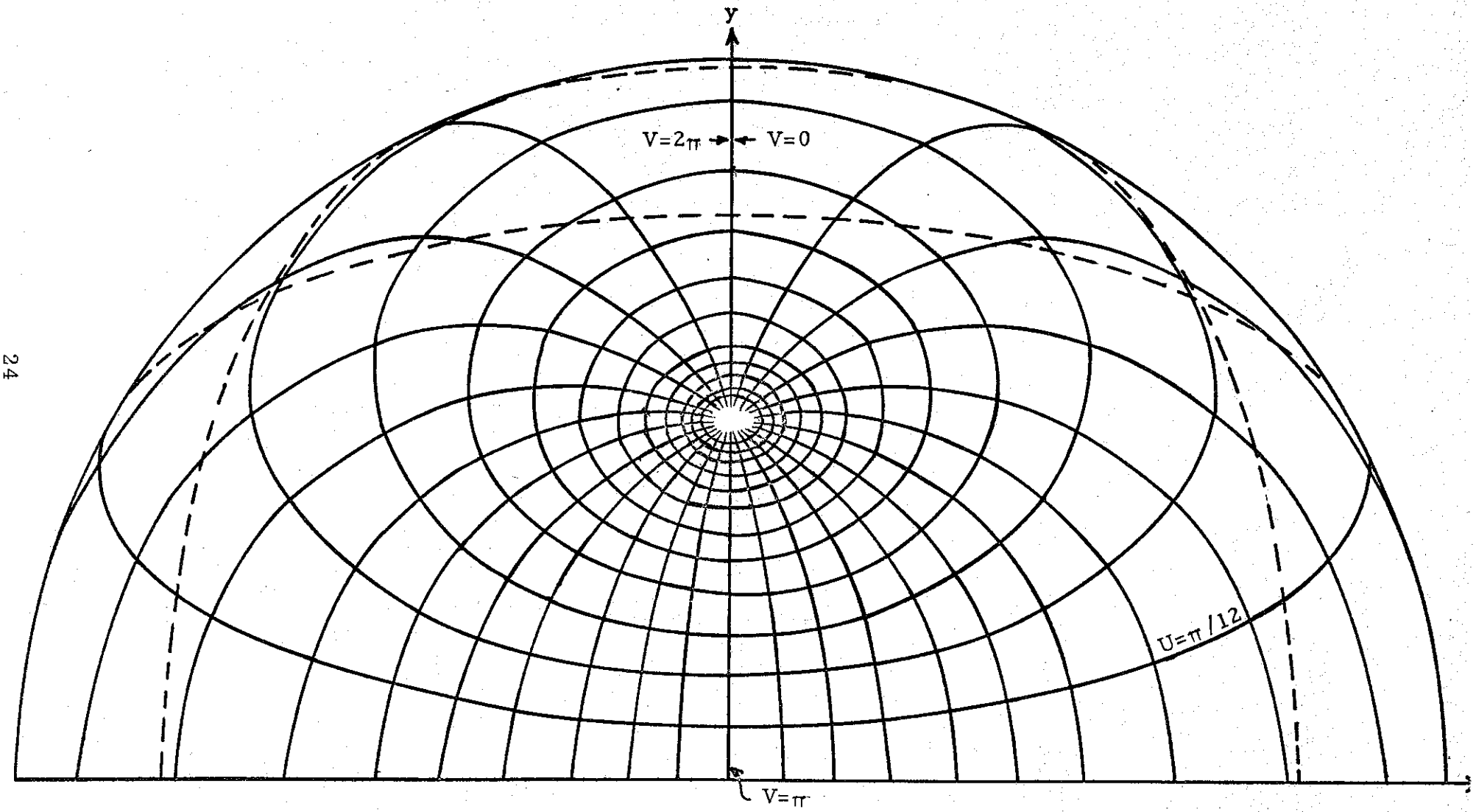

Figure 5: A view of the U-V lines for $\theta_p = 30^\circ$

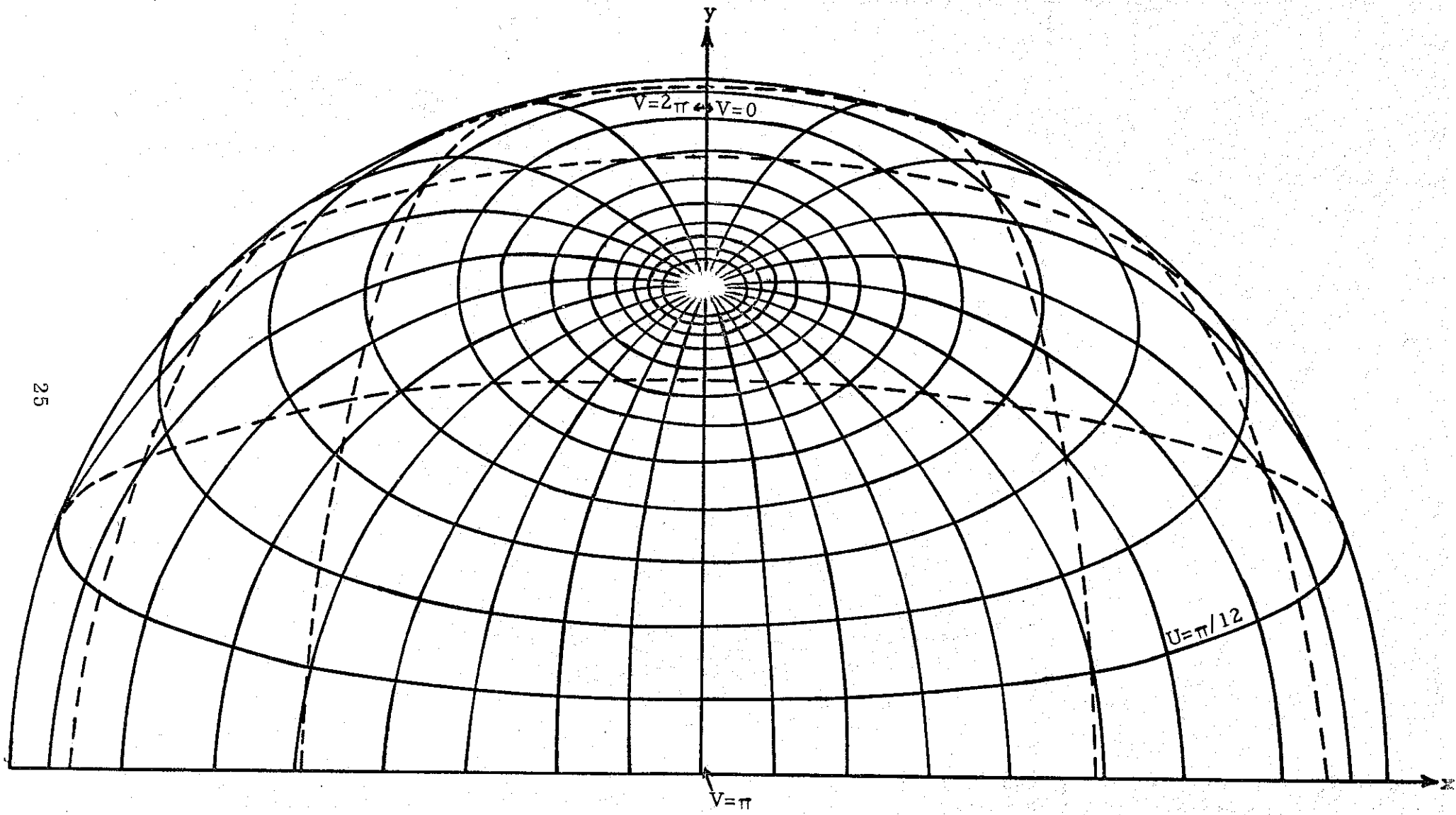

Figure 6: A view of the U-V lines for $\theta_p = 45^\circ$

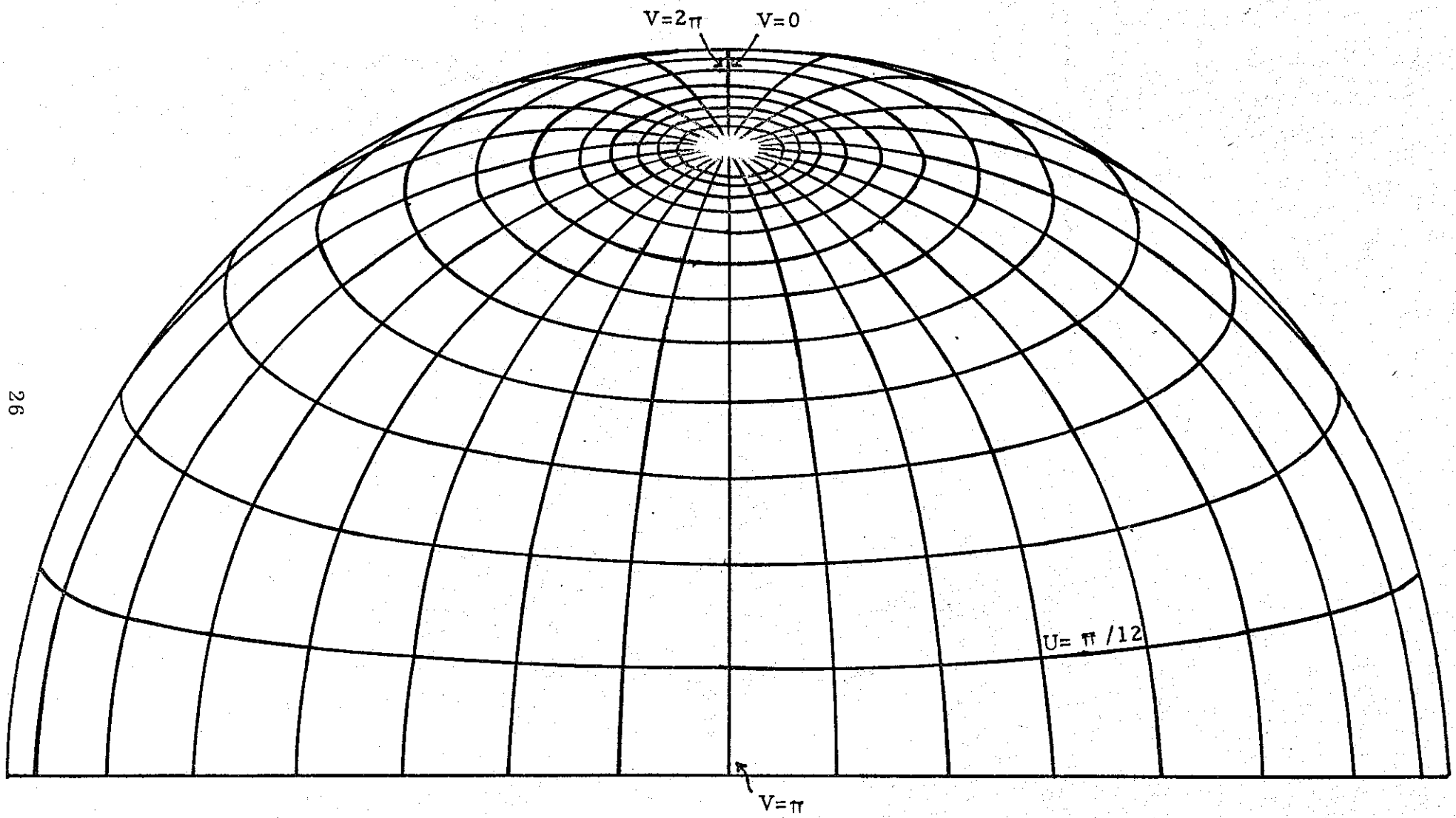

Figure 7: A view of the U-V lines for $\theta_p=60^\circ$

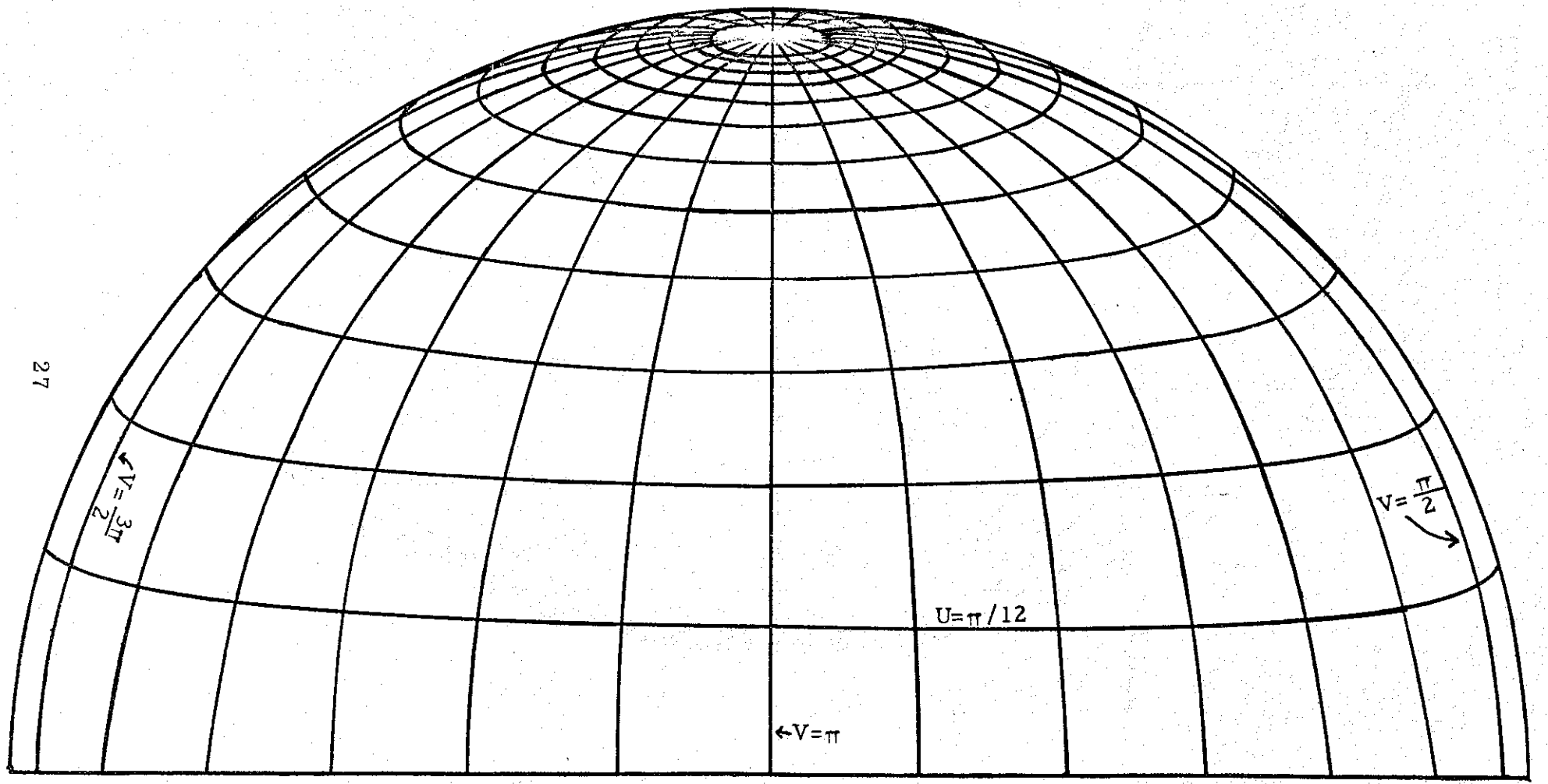

Figure 8: A view of the U-V lines for $\theta_p = 75^\circ$

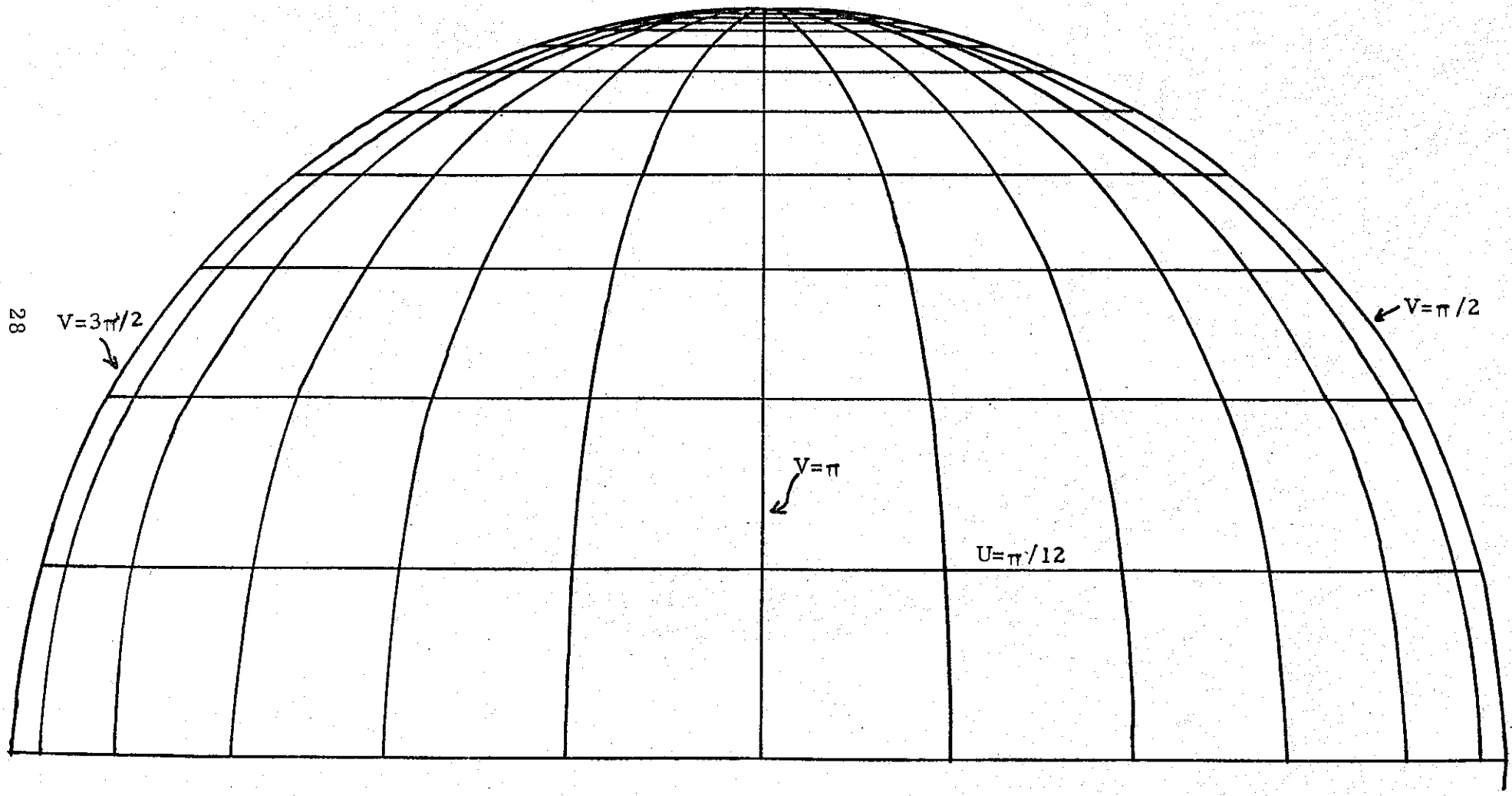

Figure 9: A view of the U-V lines for $\theta_p = 90^\circ$

$$b_v = \frac{\sin\theta_p \sin V}{\sin^2 V + \sin^2\theta_p \cos^2 V} \tag{34}$$

$$a_v = \frac{\sin\theta_p}{\sqrt{\sin^2 V + \sin^2\theta_p \cos^2 V}} \tag{35}$$

Similarly, equation (29) becomes

$$\frac{x^2}{a_v^2} + \frac{(y-y_v)^2}{b_v^2} = 1 \tag{36}$$

where

$$y_u = \frac{\sin\theta_p \sin hU \cosh U}{\sin^2\theta_p + \sinh^2 U} \tag{37}$$

$$b_u = \frac{\sin\theta_p \cos\theta_p \sinh U}{\sin^2\theta_p + \sinh^2 U} \tag{38}$$

$$a_u = \frac{\sin\theta_p}{\sqrt{\sin^2\theta_p + \sinh^2 U}} \tag{39}$$

Thus, our view of the constant U and V lines yields ellipses. This is clear a priori since we are viewing circles at an angle. The parameters of the ellipes are not clear a priori, but they are given by the above equations.

Let us examine Figures 4 to 9. The range of V is from 0 to 2π. We have plotted the constant V lines for $V = 0(\pi/12)2\pi$, i.e., at jumps of 15°. The range of U is from 0 to π. We have plotted the constant U lines for $U = 0\ (\pi/12)\pi$. The V lines are lines of electric field. The U lines can be thought of either as lines of magnetic field

or as equipotentials for the electric field. The pictures can be used for any monocone whose surface intersects a sphere along any of the constant U lines given. The corresponding monocone impedance is easily shown to be

$$Z = 60U \tag{40}$$

and its α and β angles follow from the equations

$$\tan\alpha = \tan\theta_p \coth U \tag{41}$$

$$\tan\beta = \sin\theta_p \operatorname{csch} U \tag{42}$$

A juggle of the above three equations leads back to equation (12).

In Figures 4, 5, and 6 we have plotted the continuation of the U and V lines on the back of the visible sphere as dotted lines. In the other three pictures we have not done this as it would result in too big a confusion of lines. From equation (29) we see that the U lines slop over onto the back (invisible) half of the hemisphere if

$$\tanh U < \sin\theta_p \tag{43}$$

Similarly, from equation (26), the V-lines disappear behind the edge of the visible portion of the hemisphere if

$$V < \theta_p \quad \text{or} \quad V > 2\pi - \theta_p \tag{44}$$

Another interesting point about the pictures is that, since we know that half the electric field lines fall between the $V = \pi/2$ and $V = 3\pi/2$ lines, it follows from equations (2.32) to (2.35) that half the electric field lines in the pictures fall within the circle whose center is at the origin and whose perimeter passes through the pole. The pole angle for an arbitrary monocone described by α, β parameters can be easily determined from

$$\cos\theta_p = \frac{\cos\alpha}{\cos\beta} \tag{45}$$

There are various other quantities one could calculate from the formulas already presented. We will restrict ourselves to one more the ratio of the electric field at $\theta = 0$ to the electric field at $\theta = \pi$. This ratio can be thought of as a rough measure of the effectiveness of the monocone in directing energy in the forward direction. From a differentiation of equation (29), the ratio is given by

$$\left.\frac{dU}{d\theta}\right|_{\substack{\theta = 0 \\ \varphi = \pi/2}} \Bigg/ \left.\frac{dU}{d\theta}\right|_{\substack{\theta = \pi \\ \varphi = \pi/2}} = \cot^2 \frac{\theta_p}{2}. \tag{46}$$

3. BACK RADIATION

The final topic we will treat in this section is that of back radiation, i. e., what fraction of the total power radiated is within a given solid angle in the backward direction. The total power radiated within any solid angle Ω_o is given by

$$P = \frac{1}{2} \int_{\Omega_o} (\underline{E} \times \underline{H}^*) \cdot \underline{e}_r \, d\Omega \tag{47}$$

where the integration is over a unit sphere. In terms of U and V this power can be written as

$$P = \frac{1}{2Z_o} \int_{\Omega_o} (\nabla U \times \nabla V) \cdot \underline{e}_r \, d\Omega \tag{48}$$

But, using a standard surface integral theorem (see, for example, reference 4, page 509), the above integral can be transformed to

$$P = \frac{1}{2Z_o} \int_C U \frac{\partial V}{\partial \ell} \, d\ell \tag{49}$$

---

4. Van Bladel, J., Electromagnetic Fields, McGraw-Hill Book Co., Inc., New York, 1964.

where C is the contour containing Ω_o on its left at all points and $d\ell$ is the unit of length along this contour. Within an Ω_o defined by two lines of constant U differing by ΔU and two lines of constant V differing by ΔV, equation (49) gives immediately

$$P = \frac{\Delta U \Delta V}{2Z_o} \tag{50}$$

In particular, for the total radiation, ΔU is the difference between the monocone value of U and zero, its value on the ground plane, while ΔV is 2π. But we know from equation (40) that on the monocone U is Z/60 which, from equation (12), is just $\cosh^{-1}(\sin\alpha/\sin\beta)$. Thus, with our normalization, the total power radiated, P_t, can be written as

$$2Z_o P_t = 2\pi \cosh^{-1}(\sin\alpha/\sin\beta). \tag{51}$$

Now it is quite straight forward, from equation (2.49) and our previous equations for U and V to write the power radiated in the cone contained between $\theta = \theta_b$ and $\theta = \pi$ (assuming the back radiation cone does not intersect the real monocone, i.e., that $\theta_b > \alpha + \beta$) in the following integral form

$$2Z_o P_b = \frac{1}{2} \frac{\cos\theta_p - \cos\theta_b}{1 - \cos\theta_p \cos\theta_b} \int_o^{\pi} \frac{F(\theta_p, \varphi)}{1 - F^2(\theta_p, \varphi)} \ln\left(\frac{1 + F(\theta_p, \theta)}{1 - F(\theta_p, \varphi)}\right) d\varphi \tag{52}$$

where

$$F(\theta_p, \varphi) = \frac{\sin\theta_p \sin\theta_b \sin\varphi}{1 - \cos\theta_p \cos\theta_b} \tag{53}$$

Equation (52) is in the form of a tabulated integral (reference 5, page 593) and so, carrying out the integral, substituting for θ_p in terms of α and β, and simplifying, we are led to

---

5. Gradshteyn, I. S., and I. M. Ryzhik, Table of Integrals, Series and Products, Academic Press, New York, 1965.

$$2Z_o P_b = \pi \ln \left(\frac{\cos\beta - \cos\alpha \cos\theta_b}{\cos\alpha - \cos\beta \cos\theta_b} \right) \tag{54}$$

Thus, the fractional power radiated in the cone between $\theta = \theta_p$ and $\theta = \pi$ is just

$$\frac{P_b}{P_t} = \frac{1}{2} \ln \frac{\left(\frac{\cos\beta - \cos\alpha \cos\theta_b}{\cos\alpha - \cos\beta \cos\theta_b} \right)}{\cosh^{-1}(\sin\alpha / \sin\beta)} \tag{55}$$

This is the back radiation that would occur if our monocone were infinite. Since it is attached to a structure that tends to direct even more of the energy forward (by virtue of having an effective α less than the monocone α) the actual back radiation would be somewhat less than that given by equation (55). Nevertheless, it is of interest to note that for $\theta_b = \pi/2$ and reasonable values of α and β, equation (55) predicts back radiations of the order of 10 to 20 %.

SECTION III

ZERO-NET-FLUX CAPACITOR-ARM CONFIGURATION

This section determines those positions of the four peaking capacitor arms of the pulser section such that no net flux links any pair of arms either in the charging stage, when all the return current flows through the Marx generator, or in the discharging stage, when all the return current flows in the ground plane (image conductors). These two conditions on the return current are not exact, but they are good approximations.

We will consider only the cylindrical transmission line approximation to the problem. The errors introduced by the actual tapering of the capacitor-arm spacing are small if we use a cross section near the middle of the arms as the cross section of our cylindrical line. A brief discussion of this type of error may be found in Section IV.

1. MARX RETURN CURRENT

The first case we will look at in this section is the one where the four capacitor arms carry equal currents and all the current returns through the Marx. This situation is shown in Figure 10, which also gives the rotation we will use in discussing the case.

It can be seen that what we have pictured in Figure 10 is actually an upside-down view of the Marx-capacitor-arm cross section. It is less awkward, notationally, to discuss the problem in terms of the coordinates of Figure 10 for the case when the Marx generator is present.

We will immediately assume that all currents can be replaced by line currents at some effective positions, for purposes of calculating fields. The error introduced by this assumption will be discussed briefly in Section IV. It is not great for the case we are considering.

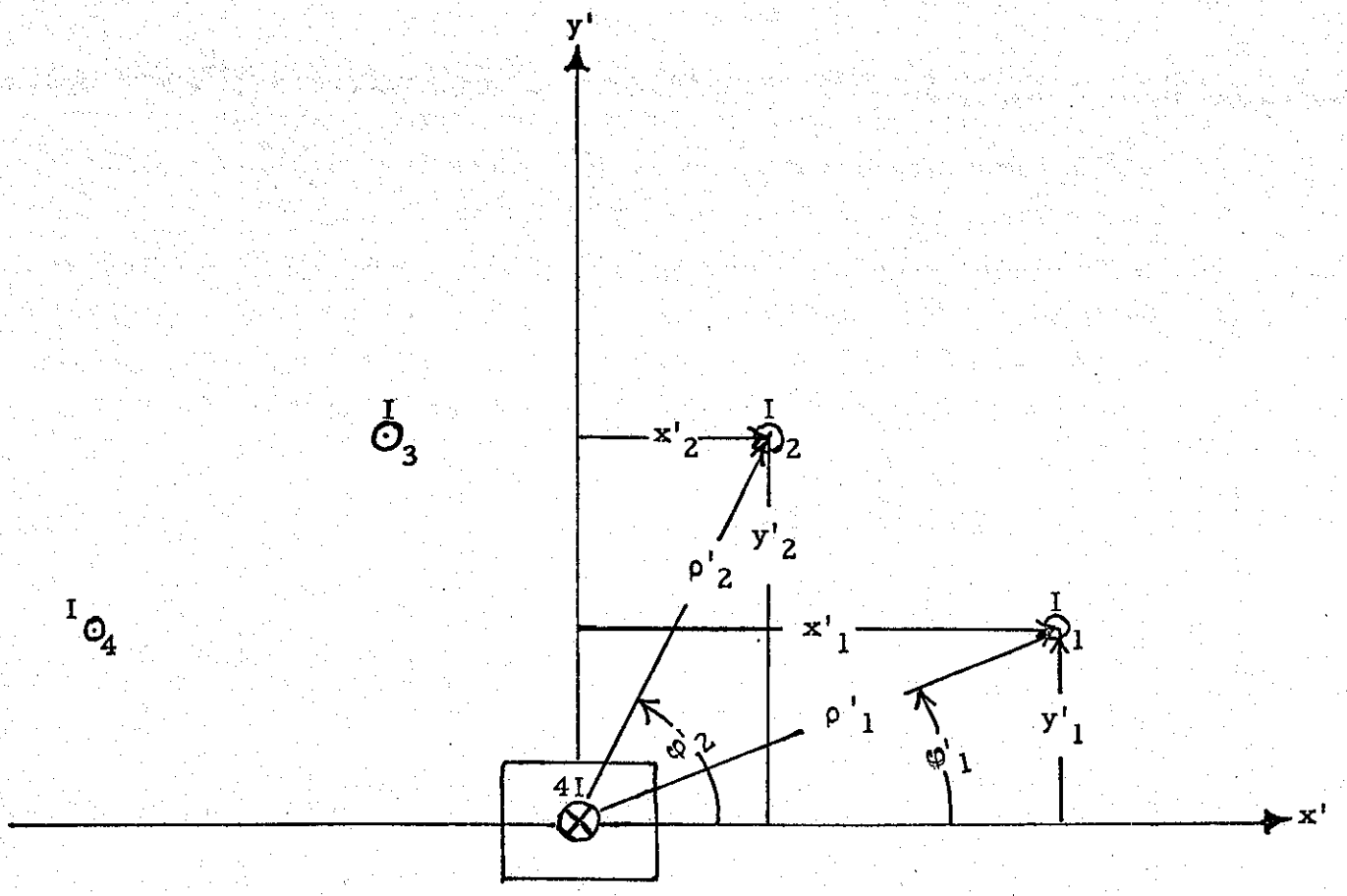

Figure 10: Zero net flux problem with Marx return

It is obvious from the physics of the problem that the zero-net-flux configurations must be symmetrical about the y-axis (i. e., the vertical plane through the Marx generator). This symmetry will automatically ensure zero net flux between arms 2 and 3 and between arms 1 and 4. If, while preserving the reflection symmetry, we manage to get zero net flux between arms 1 and 2, the symmetry ensures zero net flux between the other three pairs of arms (1-3, 2-4, 3-4).

Let us, therefore, determine the flux between arms 1 and 2 as a function of the positions of those two arms, assuming the positions of the remaining two arms to be determined from symmetry. But the flux between any two two-dimensional points at distances "a" and "b" from a line current I is just $(\mu_o I/2\pi) \ln (b/a)$, the direction being determined by the right hand rule. Thus, in Figure 10, the flux between arms 1 and 2 due to the currents in arms 1 and 2 themselves cancels. The flux between arms 1 and 2 due to the current in arm 3 is just

$$\Phi_3 = \frac{\mu_o I}{2\pi} \ln \left(\frac{d_{31}}{d_{32}} \right) \tag{56}$$

where

$$d_{31}^2 = (x'_1 + x'_2)^2 + (y'_1 - y'_2)^2 \tag{57}$$

$$d_{32}^2 = 4x'^2_2 \tag{58}$$

and the flux goes in the positive-y direction. Similarly, the flux due to arm 4 is

$$\Phi_4 = \frac{\mu_o I}{2\pi} \ln \left(\frac{d_{41}}{d_{42}} \right) \tag{59}$$

where

$$d_{41}^2 = 4x'^2_1 \tag{60}$$

$$d_{42}^2 = (x'_1 + x'_2)^2 + (y'_1 - y'_2)^2 = d_{31}^2 \tag{61}$$

and the flux due to the current in the Marx generator is

$$\Phi_m = - \frac{4\mu_o I}{2\pi} \ln\left(\frac{\rho'_1}{\rho'_2}\right) \tag{62}$$

Thus, for zero net flux between arms 1 and 2,

$$\ln\left(\frac{d_{31}}{d_{32}} \cdot \frac{d_{41}}{d_{42}}\right) = 4 \ln\left(\frac{\rho'_1}{\rho'_2}\right) \tag{63}$$

or, using previous equations for the d's

$$\frac{x'_1}{x'_2} = \left(\frac{\rho'_1}{\rho'_2}\right)^4 \tag{64}$$

This can also be written as

$$\frac{\cos\varphi'_1}{\rho'^3_1} = \frac{\cos\varphi'_2}{\rho'^3_2} \tag{65}$$

Equation (65) is the basic condition for flux cancellation with the Marx generator present. It can be seen that we can set the position of one arm (say arm 1) arbitrarily, but that once this position is set the other arm must fall along a certain line in the plane of the cross section. We see trivially that $\varphi'_2 = \varphi'_1$, $\rho'_2 = \rho'_1$ is one point on this line, and if we specify that $x'_1 \geq x'_2$ (no real restrictuion, just a definition of what we mean by arm 1 and arm 2), the trivial solution is the terminus of the line of positions of arm 2.

We can look for planar solutions of equation (64) by setting $y'_1 = y'_2 = h$, $x'_1 = \alpha_1 h$, $x'_2 = \alpha_2 h$ and obtain

$$\alpha_1^4 + 2\alpha_1^2 - \alpha_1 \frac{(\alpha_2^2 + 1)^2}{\alpha_2} + 1 = 0 \tag{66}$$

or, dividing out our known, trivial root of $\alpha_1 = \alpha_2$,

$$\alpha_2\alpha_1^3 + \alpha_2^2\alpha_1^2 + \alpha_2^3\alpha_1 + 2\alpha_2\alpha_1 - 1 = 0 \tag{67}$$

or, setting $\alpha_1 = \alpha_2 z \equiv \alpha z$, i.e. $z = x'_1/x'_2$

$$z^3 + z^2 + \left(1 + \frac{2}{\alpha^2}\right) z - \frac{1}{\alpha^4} = 0 \tag{68}$$

Equation (68) is a cubic equation for the ratio of the x' coordinates of the capacitor arms for a given x'_2/h. As such it of course possesses algebraic solutions, but these are a little messy. A table of its solution is given as Table 3. We note that, for equation (68) to have a solution for $z > 1$ (which is true by definition), the right hand side must be less than zero for $z = 1$. Thus,

$$3 + 2/\alpha^2 - 1/\alpha^4 < 0 \tag{69}$$

i.e.,

$$x'_2/h \equiv \alpha < 1/\sqrt{3} \tag{70}$$

More generally, if $y'_1 \neq y'_2$, we can still use y_1 as the unit of length and write the trajectory of arm 2, by manipulating equation (64), in the parametric form

$$x'_2 = x'_1 t^2 \tag{71}$$

$$y'_2 = \left\{x'^2_1 (t - t^4) + t\right\}^{\frac{1}{2}} \tag{72}$$

These equations have been used to plot the arm 2 trajectories of Figure 11 and 12. In these Figures, the notation is the same as that of Figure 10 and arm 2 can lie along any of the given curves if arm 1 lies at the terminus of the curve.

TABLE 3

Planar Solutions With Marx Returns

x'_2/h	x'_1/h
.001	9.993
.01	4.495
.02	3.496
.03	3.002
.04	2.684
.05	2.454
.06	2.276
.07	2.132
.08	2.011
.09	1.908
.10	1.818
.11	1.738
.12	1.667
.13	1.603
.14	1.545
.15	1.491
.16	1.441
.17	1.395
.18	1.352
.19	1.312

x'_2/h	x'_1/h
.20	1.275
.21	1.239
.22	1.206
.23	1.174
.24	1.144
.25	1.115
.26	1.088
.27	1.061
.28	1.036
.29	1.012
.30	.990
.31	.967
.32	.946
.33	.925
.34	.906
.35	.886
.36	.868
.37	.850
.38	.833
.39	.816

x'_2/h	x'_1/h
.40	.801
.41	.784
.42	.769
.43	.755
.44	.740
.45	.726
.46	.713
.47	.699
.48	.686
.49	.674
.50	.662
.51	.650
.52	.638
.53	.626
.54	.616
.55	.605
.56	.594
.57	.584
$(3)^{-\frac{1}{2}}$	$(3)^{-\frac{1}{2}}$

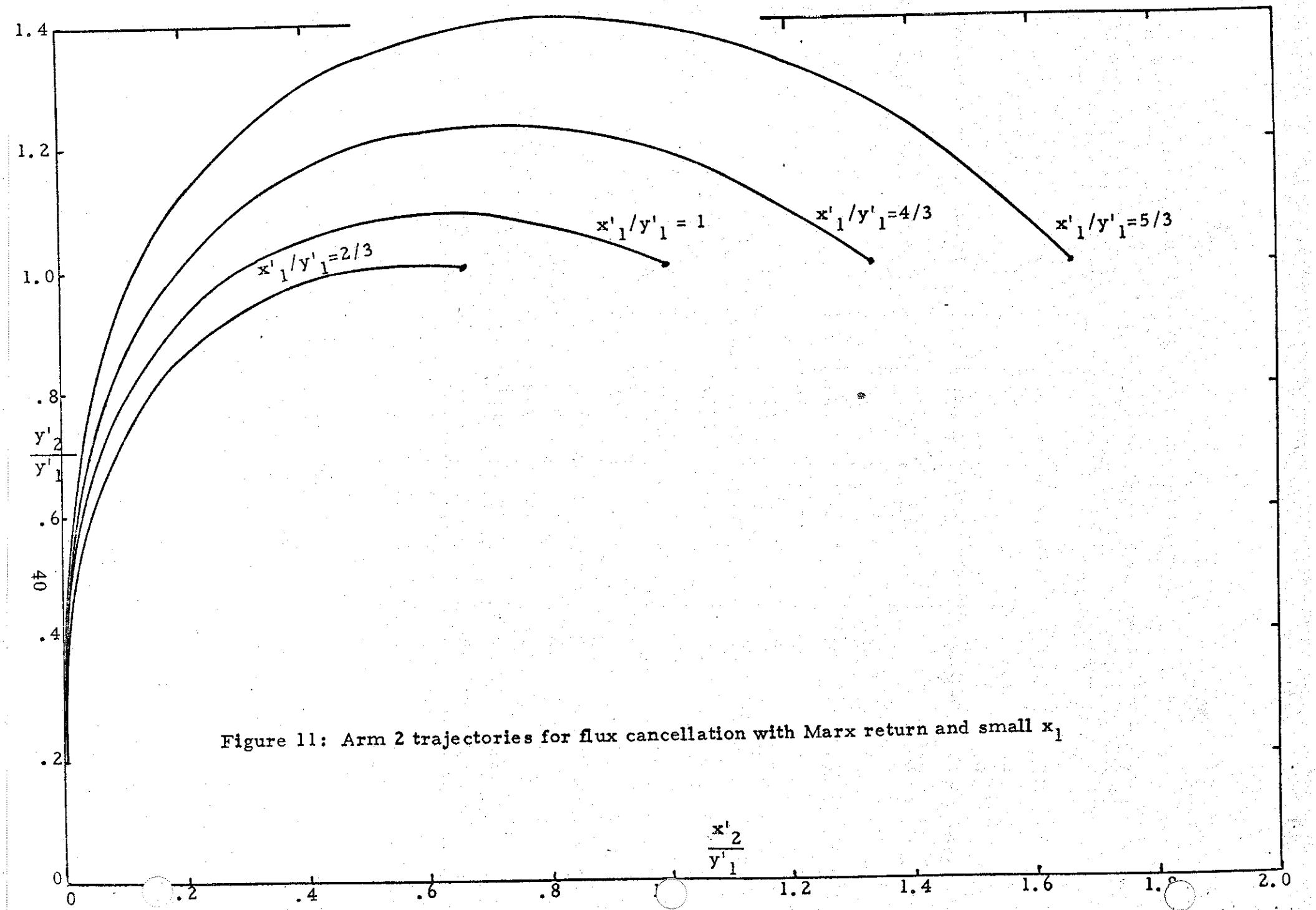

Figure 11: Arm 2 trajectories for flux cancellation with Marx return and small x_1

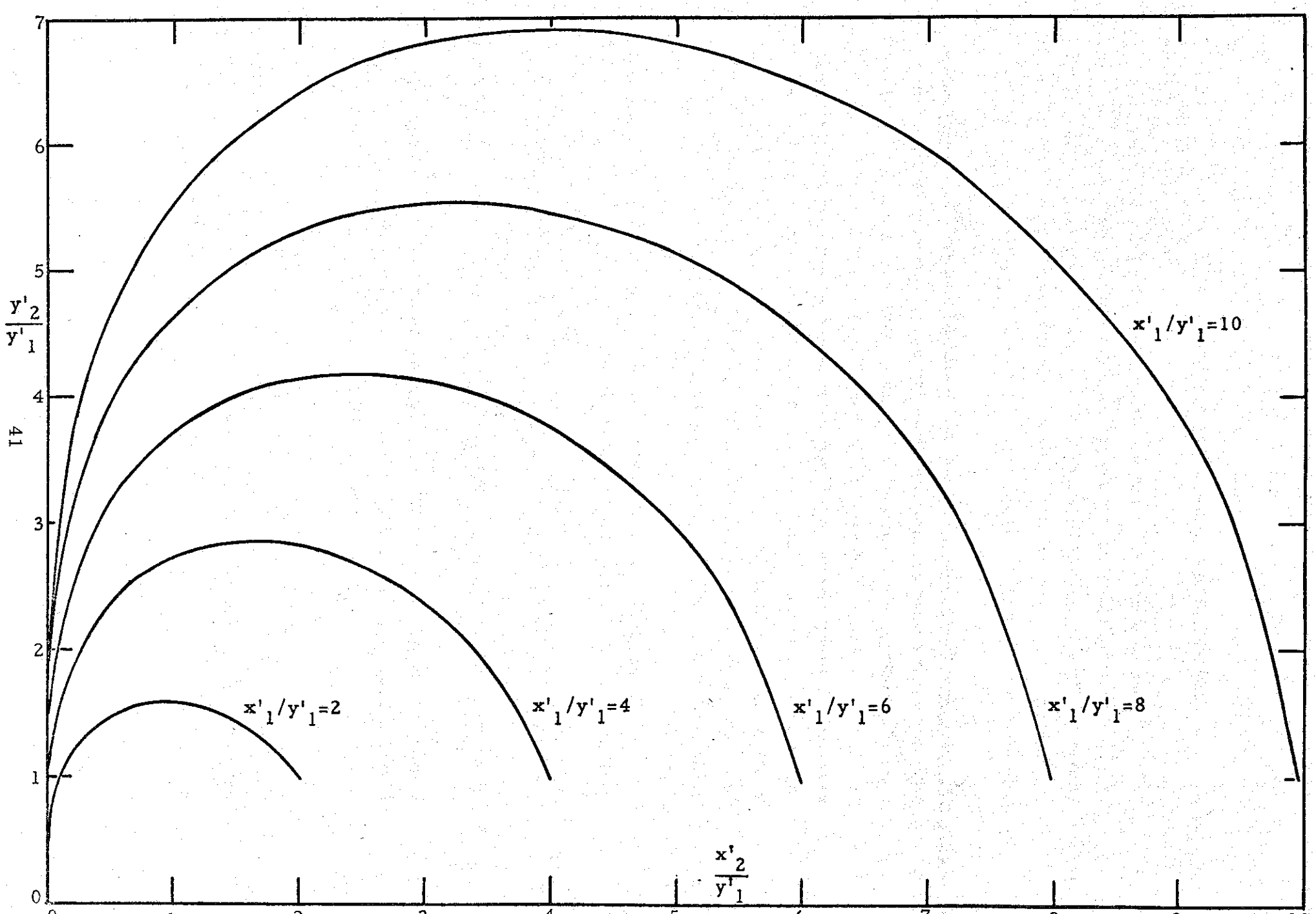

Figure 12: Arm 2 traiectories for flux cancellation with Marx return and large x,

2. IMAGE ARM RETURN CURRENT

Let us now turn to the second case of flux cancellation --the return current flowing in image conductors. The situation now is that shown in Figure 13, where we have returned to a right-side-up coordinate system. This coordinate system leads to the simplest looking equations for the present problem.

Again, symmetry about the y-axis must prevail. For this case we will determine the null-flux trajectory of arm 2 (for a given position of arm 1) by treating the completely equivalent electrostatic problem of finding the arm 2 trajectory that keeps the potentials of all arms equal while (since equal currents are assumed to flow in all capacitor arms) at the same time keeping the strengths of the line charges representing the capacitor arms equal. The electrostatic approach to the present problem will be used because some of the formulae will be useful later in calculating characteristic impedances.

In general, the potentials of arms 1 and 2 in Figure 13 are given in terms of the strengths of the line charges by

$$2\pi\epsilon_o\varphi_1 = q_1\{\ln(d_{15}/a) + \ln(d_{18}/d_{14})\} + q_2\{\ln(d_{16}/d_{12}) + \ln(d_{17}/d_{13})\} \quad (73)$$

$$2\pi\epsilon_o\varphi_2 = q_1\{\ln(d_{25}/d_{21}) + \ln(d_{28}/d_{24})\} + q_2\{\ln(d_{26}/a) + \ln(d_{27}/d_{23})\} \quad (74)$$

where "a" is the radius of the capacitor arms and the "d's" are distances between arms, the subscripts giving the particular pair of arms. Now if $\varphi_1 = \varphi_2$ and $q_1 = q_2$ the above equations can be combined to give

$$\ln d_{15} + \ln(d_{18}/d_{14}) = \ln d_{26} + \ln(d_{27}/d_{23}),$$

where we have used the obvious geometric relations $d_{25}=d_{16}$, $d_{28}=d_{17}$, etc.

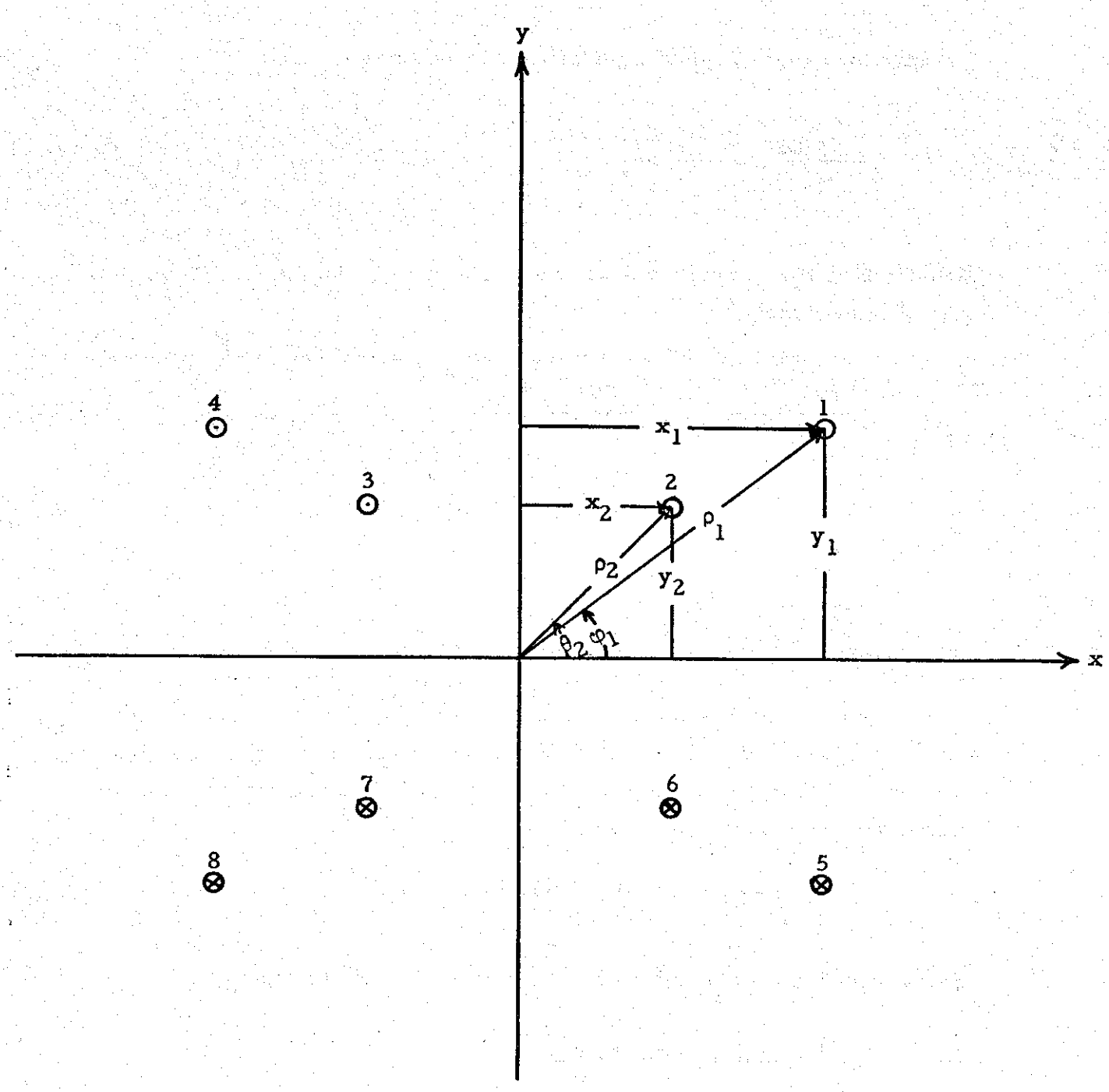

Figure 13: Zero-net-flux problem with image arms present

Taking the exponential of equation (75), we have

$$\frac{d_{15}d_{18}}{d_{14}} = \frac{d_{26}d_{27}}{d_{23}} \tag{76}$$

Substituting the coordinates shown in Figure 13, and simplifying, equation (76) becomes

$$\frac{y_1\sqrt{x_1^2+y_1^2}}{x_1} = \frac{y_2\sqrt{x_2^2+y_2^2}}{x_2} \tag{77}$$

or

$$\rho_1 \tan\phi_1 = \rho_2 \tan\phi_2 \tag{78}$$

Again, for a given position of arm 1, we have a trajectory along which arm 2 can lie and have zero net flux between any pair of the top four arms of Figure 13. There are no planar solutions of equation (77). If we again choose y_1 as the unit of length, the equation for the null-flux trajectory of arm 2 can be written as

$$x_2 = y_2^2\{1 + 1/x_1^2 - y_2^2\}^{-\frac{1}{2}} \tag{79}$$

Plots of typical trajectories are given in Figures 14 and 15.

3. COMBINED SOLUTIONS

We have now found the null flux trajectories of arm 2 for the two cases of return current. We must next find the point satisfying both null flux conditions. For a given position of arm 1 this point (if it exists at all for that particular position of arm 1) will be the intersection of two trajectories. The coordinate system we will use in finding the combined solutions is shown as Figure 16. The height of the Marx generator above the ground plane has been chosen as the unit of length.

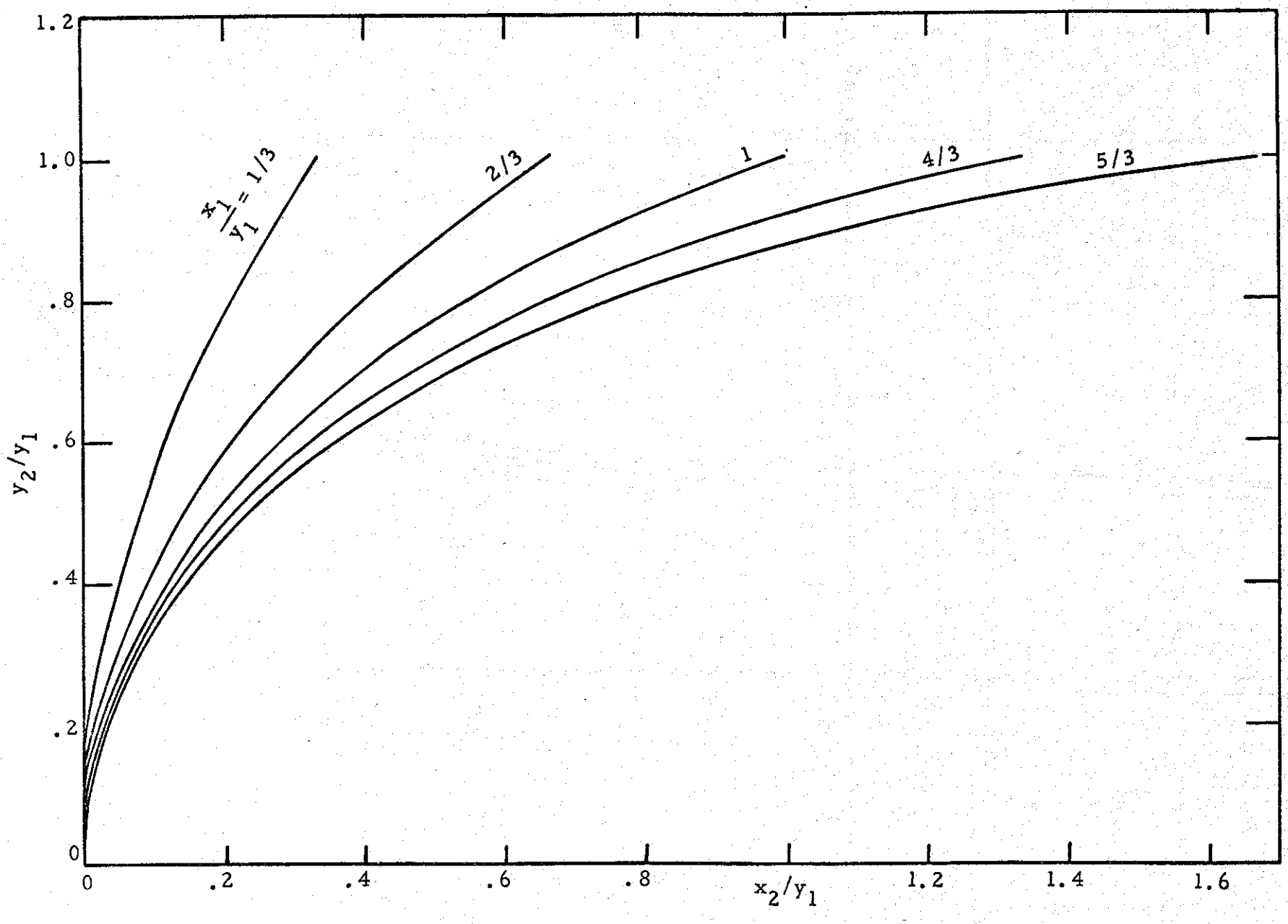

Figure 14: Arm 2 trajectories for null flux when images present and x_1 small

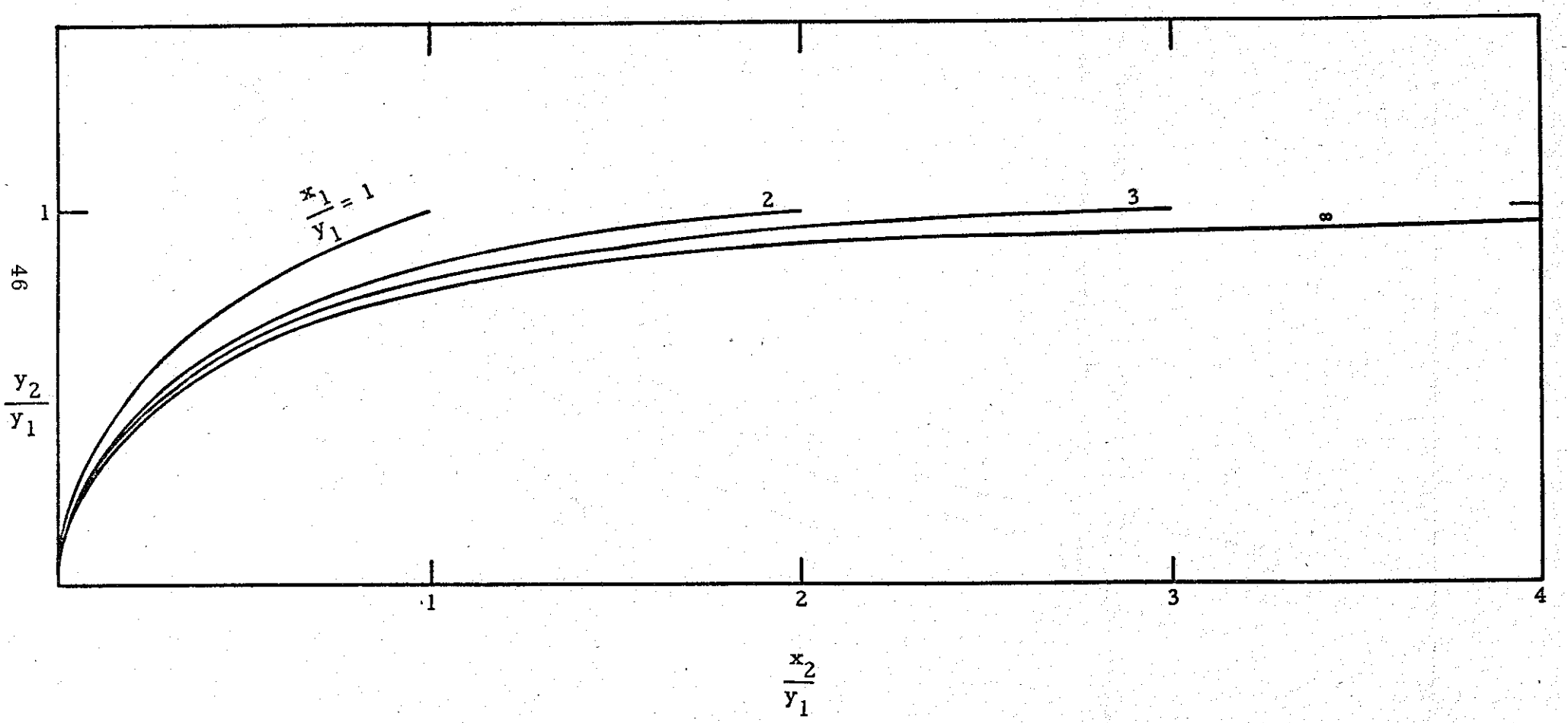

Figure 15: Arm 2 trajectories for null flux when images present and x_1 large

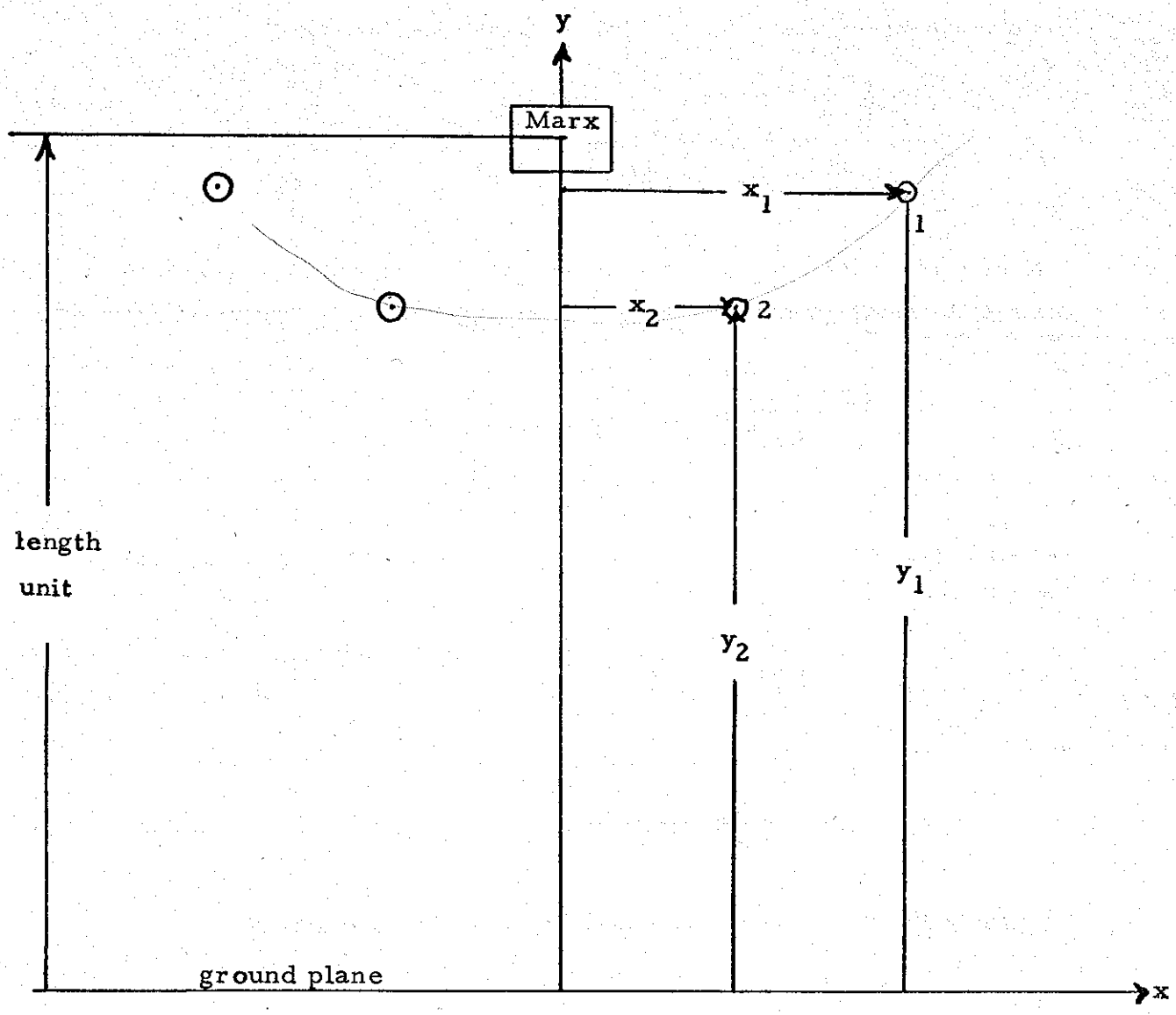

Figure 16: Coordinate system used in finding combined solutions

Let us set the position of arm 1 at(x_1, y_1). Then the null flux condition with the Marx generator carrying the return current is given, transforming equation (64) to the present notation, by

$$\frac{x_2}{\left[x_2^2 + (1-y_2)^2\right]^2} = \frac{x_1}{\left[x_1^2 + (1-y_1)^2\right]^2} \equiv g^2, \tag{80}$$

where g is defined by the position of arm 1. The null flux condition with image currents present is given, from equation (77), by

$$y_2^2 \left(1 + \frac{y_2^2}{x_2^2}\right) = y_1^2 \left(1 + \frac{y_1^2}{x_1^2}\right) \equiv f \tag{81}$$

Solving equations (80) and (81) for y_2 in terms of x_2, g, and f, we obtain

$$y_2 = 1 - \left\{\sqrt{\frac{x_2}{g}} - x_2^2\right\}^{\frac{1}{2}} \tag{82}$$

$$y_2 = \left\{\frac{-x_2^2 + \sqrt{x_2^4 + 4x_2^2 f}}{2}\right\}^{\frac{1}{2}} \tag{83}$$

Equating these (necessarily equal) values of y_2 results in

$$\left\{\sqrt{\frac{x_2}{g}} - x_2^2\right\}^{\frac{1}{2}} + \left\{\frac{-x_2^2 + \sqrt{x_2^4 + 4x_2^2 f}}{2}\right\}^{\frac{1}{2}} = 1 \tag{84}$$

By sufficient squaring and transposing, equation (84) can be changed into a polynomial equation for x_2. But this is not necessary, or even advisable, for purposes of numerical solution. The equation can be solved numerically as it stands. Once it is solved, y_2 can be determined from equation (82) or (83). Figure 17 was prepared in this manner. In preparing Figure 17 it was assumed that y_1 is between $\frac{1}{2}$ and 1

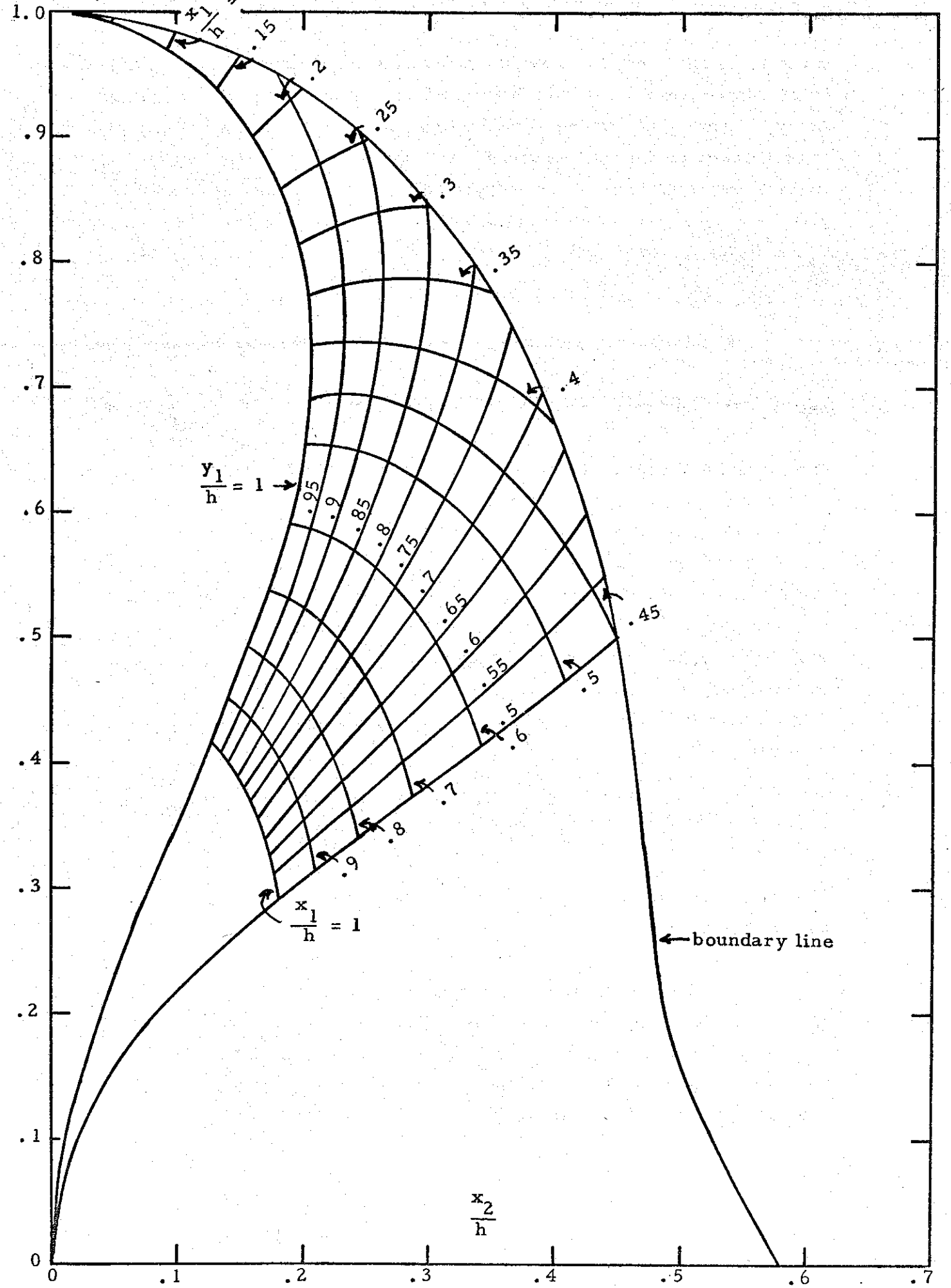

Figure 17: Arm 2 positions satisfying both null-flux conditions

while x_1 is less than 1. Any practical arm configuration should fall well within these limits. To use Figure 17 one must first decide on an x_1 and y_1. Then pick out the labled curves in the picture that correspond most closely to the real x_1 and y_1 (or extrapolate between curves for more accuracy). The intersection of the x_1-curve and the y_1-curve gives a point whose coordinates, as read from the bottom and side axes of the figure, give x_2 and y_2. For example, if x_1 is .5 and y_1 is .95 we obtain x_2 as .22 and y_2 as .65.

In Figure 17, arm 1 must lie to the right of the marked boundary line and arm 2 must lie to the left of it. The equation of the boundary line can be derived from equation (84) as follows. Equation (84) must have a solution (a trivial one) for $x_2 = x_1$. It can only have a second solution (the one of interest) if the left hand side has a negative derivative at $x_2 = x_1$, since the left hand side goes to zero at $x_2 = 0$. If the derivative were positive there must be an even number of solutions other than $x_2 = x_1$ since solutions arise from the oscillations of the left hand side about unity. From the previous trajectory plots it is clear that there is at most one interesting solution and so we are led to the negative derivative condtion. By performing the required differentiation of equation (84), setting $x_2 = x_1$ and substituting for f and g in terms of x_1 and y_1 we are led, after a little algebra, to the condition

$$x_1 \geq \left\{ \frac{(1-y_1)^2 - 6y_1^2 + \sqrt{\left[(1-y_1)^2 - 6y_1^2\right]^2 + 24y_1^2(1-y_1^2)}}{6} \right\}^{\frac{1}{2}} \qquad (85)$$

The boundary line of Figure 17 comes from taking the equality sign of this relation.

There is one more topic we must treat in this subsection and that is the determination of the characteristic impedances of the null flux configurations of Figure 17. But the characteristic impedance can be determined from the capacitance per unit length between the four arms and the ground plane by

$$\frac{Z}{Z_o} = \frac{\epsilon_o}{C} \tag{86}$$

while the right hand side of this equation is clearly given by

$$\frac{\epsilon_o}{C} = \frac{\varphi_1 \epsilon_o}{4q} \tag{87}$$

where φ_1 is the potential of arm 1 and q is the charge per unit length on each arm. Thus we find, from equations (73), (86), and (87).

$$\frac{Z}{Z_o} = \frac{1}{8\pi}\left\{\ln(d_{15}/a) + \ln(d_{18}/d_{14}) + \ln(d_{16}/d_{12}) + \ln(d_{17}/d_{13})\right\} \tag{88}$$

Substituting in this equation the values of the d's in terms of x_1, y_1, x_2, y_2 and using the height of the Marx generator, h, as a length unit for these quantities we are led quickly to

$$Z = 15 \ln(h/a) + Z_e \tag{89}$$

where Z_e, the part of the impedance depending on the relative positions of the capacitor arms, is given by

$$Z_e = 15\ln 2y_1 + 7.5 \ln\left\{1 + \left(\frac{y_1}{x_1}\right)^2\right\}\left\{\frac{(x_1-x_2)^2 + (y_1+y_2)^2}{(x_1-x_2)^2 + (y_1-y_2)^2}\right\}\left\{\frac{(x_1+x_2^2) + (y_1+y_2)^2}{(x_1+x_2)^2 + (y_1-y_2)^2}\right\} \tag{90}$$

Equation (89) should be easy to use when h, a, x_1, and y_1 are decided upon. The value of h in the real case can be taken as the height of the center of the Marx generator about the ground plane and "a" is the effective radius of the capacitor arms. Specifying x_1 and y_1 determines x_2 and y_2 by the null flux condition, and so Ze can be thought of as a function of x_1 and y_1 alone for the configurations we are interested in. Numerical values of this function are given in Table 4.

TABLE 4

Ze-configuration dependant poart of capacitor arm characteristic impedance

x_1 \ y_1	1	.95	.90	.85	.80	.75	.70	.65	.60	.55	.50
.05	184.3										
.10	143.2										
.15	119.3										
.20	102.7	123.3									
.25	90.3	98.2	141.6								
.30	80.3	84.1	91.4	124.7							
.35	72.2	74.0	76.8	81.9	95.4						
.40	65.4	66.2	67.1	68.8	71.1	76.0	89.3				
.45	59.6	59.6	59.6	59.7	60.0	60.5	61.4	63.2	66.8	73.9	
.50	54.6	54.2	53.7	53.0	52.3	51.4	50.5	49.5	48.4	46.9	45.2
.60	46.4	45.5	44.4	43.1	41.6	39.9	38.0	35.9	33.4	30.7	27.6
.70	40.1	38.9	37.5	36.0	34.3	32.4	30.3	27.9	25.4	22.5	19.4
.80	35.1	33.7	32.3	30.7	28.9	27.0	24.8	22.5	20.1	17.4	14.4
.90	31.1	29.7	28.2	26.6	24.8	22.9	21.2	18.7	16.3	13.8	11.1
1.00	27.8	26.5	25.0	23.4	21.7	19.8	17.9	15.8	13.6	11.3	8.7

SECTION IV

DISCUSSION OF SOME DETAILS

In this section we will pick up half a dozen loose ends that have been left hanging up to now because of our primary purpose of getting to final results and presenting data with as much dispatch as possible. Each of the following six paragraphs discuss one of these loose ends.

First, in the analysis of Section II we have assumed an infinite flat fround plane. Real construction limitations may require the ground plane in the neighborhood of the apex of the cone to be somewhat tilted. (we are not speaking here of the general slope mentioned in Section II, but of a much smaller region near the apex). The ground plane may have to be perpendicular to the axis of the monocone near its apex. Nevertheless, the transverse extent of the perturbation of the ground plane should be quite a bit less than the length of the monocone and so the overall characteristics we have calculated (impedance, field distributions) should be accurate. Our neglect of the perturbation of the ground plane is no more serious than the other idealizations that were necessary to make the analysis at all tractable.

Second, the finite cross sections of the conductors carrying the current in peaking capacitor section of the pulser have been neglected in the analysis of Section III. We have assumed line currents. The most serious consequence of this assumption would be in the calculation of the field due to the current in the Marx generator in Section III. 1. But even in this case, a simple analysis shows that the relative error in the flux between arms 1 and 2 due to the Marx current is at most of order $(m/r_1)^2/\ln(r_1/r_2)$, where m is the effective radius of the cross-section of the Marx, as long as we choose the "effective position" of the line current representing the Marx current to be at the geometrical center of its cross section. Even this relative error is of order 10% or less but this is further reduced by the fact that the current in the Marx is, at least approximately, uniformly distributed about its axis and for axially symmetric current distributions there is no error at

all in calculating the fields by assuming the entire current to flow in a line along the axis.

Third, we were faced with a problem in calculating the characteristic impedance of the capacitor arm section in Section III. 3. The arms do not really form a cylindrical transmission line since they must taper apart as they go from the monocone to the upper transition section, and yet they do not form a conical line since the arms themselves are of uniform radius along their length. The calculation was made by assuming a cylindrical line whose cross section is the same as that of the real line at some point (say half way) along its length. This seems to be a good assumption for at least two reasons. One reason is that no matter what point along the line we calculate the impedance at (i. e., no matter which point along the line we choose to define h, the height of the Marx in equation (89)) we obtain, for the kinds of geometries and impedance levels contemplated, an impedance within 3. 5% of the value calculated at the half way point. Another reason is that, if we define a conical line by tapering the arm radii as well as their spacing from the midpoint of the arms back to an apex, we obtain an impedance within 4% of that calculated under our cylindrical line assumption.

Fourth, the capacitor arm radii are not too well defined because these arms are not perfectly conducting rods. We should really speak of an "effective" radius of the capacitor arms. But the effective radius should approximate the geometric radius (it will be a little smaller) and an error of even 20% in estimating this parameter will result in an error (when used in equation (89)) of less than 2% in the impedance of a 140-ohm line.

Fifth, we have spoken little of minimizing the dispersion due to the transitions between the various sections of the pulser and simulator except for our overall, and necessary, criterion of uniform characteristic impedance along the line. In addition, we should minimize the difference in curvature of the wavefronts on the various sections by sloping each section as little as is consistent with other requirements.

(eventually we are feeding into the zero-slope parallel-plate region). We had this in mind in our discussions of the field lines in Section II. 2. As a minimum, we should try to keep the length along the upper conductor, up to the parallel-plate region, within ten feet of the length of the ground plane up to the parallel-plate region.

Last, imperfect impedance matches between the various sections of the pulser and simulator will change the input impedances slightly from the characteristic impedances that have been calculated in this report. But this is precisely the effect that will be minimized by keeping the characteristic impedance uniform throughout the structure. From the data presented in Sections II and III, it should be possible to arrange a pulser geometry such that mismatches between its sections are well below an acceptable level.

REFERENCES

1. Schelkunoff, S. A., Advanced Antenna Theory, John Wiley and Sons, Inc., New York, 1952.

2. Smythe, W. R., Static and Dynamic Electricity, McGraw-Hill Book Co., Inc., New York, 1950.

3. Baum, C. E., "The conical transmission line as a wave launcher and terminator for a cylindrical transmission line", AFWL Sensor and Simulation Notes, Note 31, January 1967.

4. Van Bladel, J., Electromagnetic Fields, McGraw-Hill Book Co., Inc., New York, 1964.

5. Gradshteyn, I. S., and I. M. Ryzhik, Table of Integrals, Series, and Products, Academic Press, New York, 1965.